



HAL
open science

Titan's Induced magnetosphere from plasma wave, magnetic field and particle observations

Ronan Modolo, Norberto Romanelli, Cesar Bertucci, Jean-Jacques Berthelier, Patrick Canu, R. Piberne, Andrew Coates, Francois Leblanc, Niklas Edberg, Michiko Morooka, et al.

► **To cite this version:**

Ronan Modolo, Norberto Romanelli, Cesar Bertucci, Jean-Jacques Berthelier, Patrick Canu, et al.. Titan's Induced magnetosphere from plasma wave, magnetic field and particle observations. 2020. <hal-05568651>

HAL Id: hal-05568651

<https://hal.science/hal-05568651v1>

Preprint submitted on 26 Mar 2026

HAL is a multi-disciplinary open access archive for the deposit and dissemination of scientific research documents, whether they are published or not. The documents may come from teaching and research institutions in France or abroad, or from public or private research centers.

L'archive ouverte pluridisciplinaire **HAL**, est destinée au dépôt et à la diffusion de documents scientifiques de niveau recherche, publiés ou non, émanant des établissements d'enseignement et de recherche français ou étrangers, des laboratoires publics ou privés.



Distributed under a Creative Commons CC BY-NC-ND 4.0 - Attribution - Non-commercial use - No Derivative Works - International License

Titan's Induced magnetosphere from plasma wave, magnetic field and particle observations

R. Modolo¹, N. Romanelli^{2,3}, C. Bertucci⁴, J.-J. Berthelier¹, P. Canu⁵, R.
Piberne⁵, A.J. Coates⁶, F. Leblanc¹, N. J. T. Edberg⁷, M. Morooka⁷, M.
Holmberg⁸, E. Dubinin⁹, L. Regoli¹⁰, W.S. Kurth¹¹, D.A. Gurnett¹¹, J.-E.
Wahlund⁷, H. Waite¹² and M.K. Dougherty¹³

¹LATMOS / UVSQ / SU / CNRS, 11 bd d'Alembert, 78280 Guyancourt, France

²NASA Goddard Space Flight Center, Greenbelt, Maryland, USA

³CRESST II, University of Maryland, Baltimore County, USA

⁴Institute for Astronomy and Space Physics - IAFE, Ciudad Universitaria, Buenos-Aires, Argentina

⁵LPP-Ecole Polytechnique, 91128 Palaiseau Cedex, France

⁶MSSL University College London, Holmbury St Mary, Dorking RH5 6NT, UK

⁷IRF, Box 537, SE-75121 Uppsala, Sweden

⁸European Space Agency - ESTEC, 1 Kepleeran, Noordwijk, The Netherlands

⁹Max Planck Institute, MPS, Gottingen, Germany

¹⁰Johns Hopkins University Applied Physics Laboratory, Laurel, Maryland, USA

¹¹The University of Iowa, Dept of Physics and Astronomy, Iowa City, USA

¹²Southwest Research Institute, San Antonio, Texas, USA

¹³Imperial College of Science, Technology and Medicine, Space and Atmospheric Physics Group,
Department of Physics, London SW7 2BW, UK

Key Points:

- We analyze Titan's induced magnetosphere making use of CASSINI RPWS, CAPS and MAG measurements from 82 flybys
- We derive the first global electron density map of Titan's near environment, that ranges between 10^{-2} to 10^3 cm^{-3} , delimiting an average induced magnetosphere standoff distance of $1.85 R_T$ and $2.77 R_T$ on the ram and flank direction respectively.

- 28 • We identified ionospheric ions with energies between 10 eV to 3 keV, increasing
29 along the convective electric field direction, with an intensity of 0.7 mV/m, con-
30 sistent with an average estimate of 0.61 mV/m deduced from $|\vec{v} \times \vec{B}|$ calculation.

31 **Abstract**

32 Cassini plasma wave and charged particle observations are combined with magnetome-
 33 ter measurements to investigate Titan’s induced magnetosphere. Electric field emissions
 34 close to Titan are identified as upper hybrid resonance emissions, which provide a den-
 35 sity estimate of Titan’s cold plasma. These observations have been combined with elec-
 36 tron spectrometer measurements to build an integrated map of electron density in Ti-
 37 tan’s near environment using observations from TA to T82 flybys, *ie* which includes fly-
 38 bys from the Cassini prime, equinox and part of the solstice mission. We identify a dense
 39 ionospheric region and an extended plasma wake with values ranging between 10^{-2} and
 40 10^3 cm^{-3} . Upstream of the induced magnetosphere, the presence of pickup ions in the
 41 positive hemisphere of the kronian plasma convective electric field are detected. The mass
 42 of the observed pickup corresponds to methane group ions, N_2^+ and $HCNH^+$ ions as
 43 well as Titan’s protons and molecular hydrogen ions. These ions are progressively ac-
 44 celerated by the kronian background electric field and we estimate its intensity by re-
 45 constructing the energization of this population. We find values on the order of 0.7 mV/m
 46 , consistent with an average estimate of 0.61 mV/m deduced from $\sim |\vec{V} \times \vec{B}|$ compu-
 47 tation.

48 **1 Introduction**

49 Titan’s interaction with the ambient plasma in Saturn’s magnetosphere has been
 50 categorized as atmospheric, like the ones for Mars, Venus and comets with the solar wind
 51 (Barabash, 2012). Titan’s atmosphere is partly ionized, leading to the formation of an
 52 ionosphere, which acts as an obstacle against the magnetospheric plasma flow. This con-
 53 ductive obstacle deflects the incoming flow and twists the magnetic field around the body
 54 and leading to a draped field line region, mostly populated by ionospheric or exospheric
 55 plasma, called the induced magnetosphere, as illustrated by Waite et al. (2004, Figure
 56 7). Reviews on Titan’s ionosphere, composition and its induced magnetosphere have been
 57 presented in Cravens et al. (2010) and Wahlund et al. (2014).

58 Cassini has revealed a highly variable and dynamic upstream plasma environment
 59 largely influenced by the complex nature of Saturn’s magnetosphere and its magnetodisk
 60 (Arridge, Achilleos, & Guio, 2011; Arridge, André, Bertucci, et al., 2011; Arridge, André,
 61 McAndrews, et al., 2011; Arridge, 2012). As a result, efforts on the characterization and
 62 categorization of the upstream plasma properties of the magnetic field (Bertucci et al.,

2009; Simon et al., 2013), electron distribution function (Rymer et al., 2009) and plasma density variation (Morooka et al., 2009) have been carried out. Indeed, Bertucci et al. (2009) have shown that the magnetic field at the orbit of Titan has a large variability and is affected by several factors, such as the presence of Saturn’s magnetodisk. Consequently, Titan is exposed to different magnetic orientations going from North-South to planetward field lines, to highly perturbed fields, when Titan is inside Saturn’s current sheet. Large fluctuations of the magnetospheric configuration are commonly observed between the inbound and outbound portions of passes, that occur over periods of a few minutes up to several hours, and thus affect the external draping of the magnetic field lines around Titan (Simon et al., 2010). While (Edberg et al., 2015) have presented ionospheric density map, below 2400 km, based on Langmuir Probe observations, a characterization of the electron density inside Titan’s magnetosphere is thus of interest.

Pickup ions have been observed in the vicinity of various bodies in the Solar System such as comets, Mars, Titan, Moon, Enceladus (e.g., Coates et al., 1989, 1993; Dubinin et al., 1993, 2006; Hartle et al., 2006; Yokota et al., 2009; Tokar et al., 2008). At Titan, pickup ions have been observed by Voyager 1 (Hartle et al., 1982) and Cassini (e.g., Hartle et al., 2006). These ions have large masses around 16 amu or more and arise from the ionization of Titan’s upper atmosphere and they are embedded in the magnetospheric flow. When picked-up by the magnetospheric flow they are accelerated by the motional electric field $\vec{E} = -\vec{v} \times \vec{B}$, where \vec{v} is the plasma bulk velocity and \vec{B} the local magnetic field, providing an ion escape mechanism responsible for the erosion of Titan’s atmosphere.

In this work we further characterize this unique environment making use of Magnetometer (MAG) measurements (Dougherty et al., 2004), particle data (CAPS) (Young et al., 2004) and Radio and Plasma Wave Science (RPWS) observations (Gurnett et al., 2004), providing an overall and organized description of the electron plasma environment of Titan and the pickup ion distribution. Based on such results, we also estimate the convective electric field intensity responsible for such ion population. In section 2, we introduce the approach to combine both particle and wave data to build a continuous electron density profile for each flyby of Cassini prime, equinox and the beginning of the solstice mission. The global image of the electron density in the near region of Titan is presented and discussed in section 3. Section 4 is dedicated to the description of the pickup ion population through its energy signature, mass composition and its organization with

96 respect to the ambient electric field. A discussion on the energization of these pickup ions
 97 completes this section while section 5 summarizes the main conclusions of this work.

98 **2 Measurements and methodology**

99 RPWS observations can be used to measure the electron number density of the ther-
 100 mal plasma close to Titan. Information derived from these wave electric fields data and
 101 from Langmuir probe (LP) provide two independent density estimates for the cold plasma.
 102 This study we have mainly used electron number density derived from waves emissions.
 103 Electrostatic emissions have been detected in the range from 1 to several hundreds of
 104 kHz. The most intense and structured emissions occur at the upper hybrid frequency,
 105 $f_{UH} = \sqrt{f_c^2 + f_p^2}$, with f_p the plasma frequency and f_c the electron cyclotron frequency.
 106 In Titan's vicinity, given the relatively weak magnetic field strength, the electron cyclotron
 107 frequency is much smaller than the electron plasma frequency ($f_c \ll f_p$), so the upper
 108 hybrid frequency is essentially equal to the electron plasma frequency and f_{UH} provides
 109 a direct visualization of electron density profiles. Most of the Titan flybys exhibit f_{UH}
 110 signatures either on the Medium Frequency Receiver (MFR) or on the High Frequency
 111 Receiver (HFR) and electron densities estimated by this method are in excellent agree-
 112 ment with previously published LP data (Edberg et al., 2010).

113 Electron Spectrometer observations of the Cassini Plasma Spectrometer (CAPS-
 114 ELS) are used to compute the electron number density in Saturn's magnetosphere and
 115 Titan's environment. CAPS-ELS measures suprathermal electrons distribution in the
 116 energy range from 0.6 eV to 28 keV with an energy resolution of 17% and an angular
 117 resolution of 20°. Moments, and particularly the density, are determined based on the
 118 work of Lewis et al. (2008).

119 CAPS-ELS moment calculation underestimate electron density in the cold plasma
 120 region since only part of the electron distribution function is seen due to a negative space-
 121 craft potential and also due to a relatively coarse energy discretization table below 1eV.
 122 On the other hand, f_{UH} signatures are not observed below 1-5 kHz (corresponding to
 123 0.01-0.3 cm⁻³). While the particle instrument is well designed for hot and tenuous plasma,
 124 the wave instrument is very well adapted to measured cold and dense plasma. The ex-
 125 cellent complementarity of the two data set is illustrated in Figure 1.

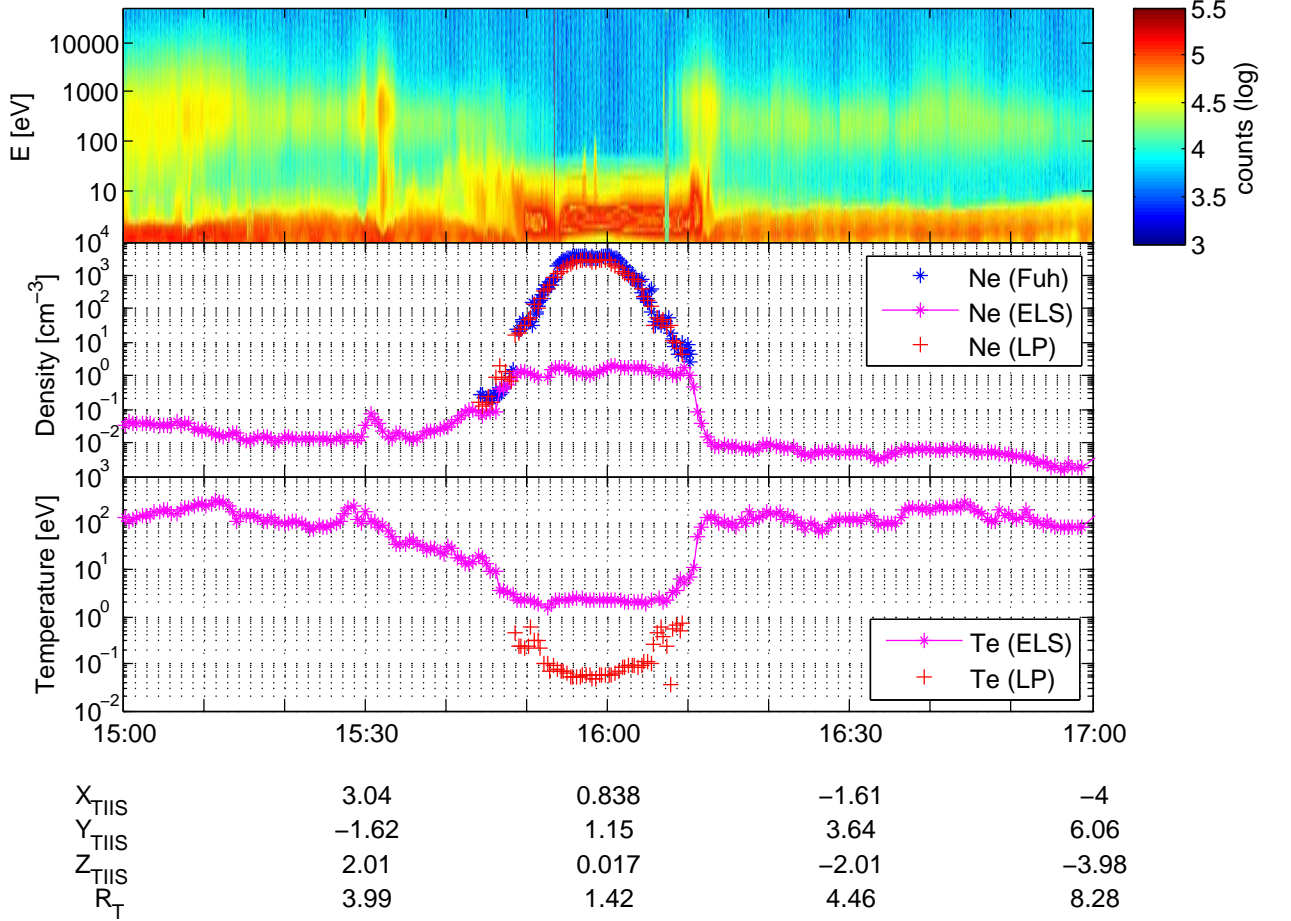


Figure 1. CAPS-ELS and RPWS observations for T20 flyby (2006 /10/25). Top panel shows CAPS-ELS Anode 5 observations. Middle panel presents electron number density estimated by CAPS-ELS moment calculation (magenta marks), LP analysis (red marks) and deduced from wave observations (blue marks). Bottom panel shows electron temperature estimated by ELS (magenta marks) and LP analysis (red marks).

126 Figure 1 shows electron density and temperature profiles retrieved from different
 127 techniques and instruments for the T20 flyby (2006/10/25). We present data in the Ti-
 128 tan interaction coordinate system (TIIS) where the positive X-axis is defined by the di-
 129 rection of the ideal co-rotational kronian plasma flow and the Y-axis points toward Sat-
 130 urn. The Z-axis completes the right handed coordinate system.

131 everal regions with different plasma regimes are crossed during this Cassini flyby.
 132 The spacecraft is first located in Saturn’s magnetosphere, characterized by a density range
 133 of $0.01\text{-}0.1\text{ cm}^{-3}$ and an electron temperature of $\sim 100\text{ eV}$. As Cassini approaches Ti-
 134 tan’s ionized environment, the electron number density progressively increases, while the
 135 electron temperature decreases. Titan’s ionosphere is clearly identified by a high elec-
 136 tron density, a low electron temperature and the signature of ionospheric photoelectrons
 137 in the CAPS-ELS spectra (Coates, 2009). In the ionospheric region, the electron den-
 138 sity deduced from LP data and f_{UH} are almost identical. The closest approach occurred
 139 at an altitude of 949 km at 15:51 SCET. The outbound leg is relatively symmetric to
 140 the inbound one, both in terms of regions crossed and global plasma parameter trends.

141 On all flybys analyzed (up to T82), a good correspondance between the density es-
 142 timated from CAPS-ELS and RPWS is observed most of the time between $0.1\text{ - }1\text{ cm}^{-3}$
 143 density interval, as illustrated in figure 1. When both RPWS and CAPS-ELS measure-
 144 ments were present during the same time interval, RPWS measurements were system-
 145 atically preferred since they provide directly the electron density through the plasma fre-
 146 quency.

147 MAG observations are used to derive information about the background magnetic
 148 field environment in the vicinity of Titan, to quantify its variability and also to empha-
 149 size the bipolar tail region reported by Simon et al. (2014).

150 CAPS-IMS observations have also been used to derive information on the ion pop-
 151 ulation, in particular the mass composition of the plasma for specific time intervals (see
 152 section 4.2). CAPS-IMS samples ions in 8 angular sectors each of them having an iden-
 153 tical field of view (FOV) of $8^\circ \times 20^\circ$. "Singles" data correspond to energy-per-charge
 154 (E/Q) spectra ranging from 1eV to 50 keV with a spectral resolution of 17%. The elec-
 155 trostatic analyzer is scanned 8 sweeps, each 4.0 s long and with 64-step energy steps, re-
 156 ferred as a A-cycle lasting 32.0 s. CAPS-ELS and IMS sensors are mounted on a rotat-
 157 ing platform capable of sweeping the CAPS instrument by $\sim 180^\circ$ around an axis par-

158 allel to the spacecraft Z-axis in about 3 min 30s. The Time-Of-Flight (TOF) analyzer
 159 is used to infer detailed compositional analysis in a so called B-cycle. During the B-cycle,
 160 the 8 angular sectors are summed together and the 64 energy steps are collapsed to 32
 161 energy steps. The B-cycle lasts 256 s. More detailed information of CAPS-IMS are pre-
 162 sented in Young et al. (2004); Hartle et al. (2006); Sittler et al. (2010).

163 **3 Electron density maps**

164 CAPS-ELS and RPWS electron density estimates are combined to provide a unique
 165 and continuous electron density profile going from Saturn’s magnetosphere to Titan’s
 166 ionosphere, for each flyby. All flybys from TA to T82 have been analyzed with the ex-
 167 ception of T7 / T73, T9 and T32, for which no data have been recorded, or a significant
 168 deviation from the ideal co-rotation flow has been emphasized (e.g., Szego et al., 2007)
 169 or the flyby occurred in Saturn’s magnetosheath. In each case, the upper hybrid line has
 170 been digitalized with the ViTos vizualization tool which display the MFR/HDR spec-
 171 trum for each acquisition. On each wave spectrum, the ViTos tool proposes the frequency
 172 of maximum wave intensity; we have confirmed the selected frequency, or we have re-
 173 selected manually a new frequency, as the f_{UH} emission frequency. Only data with a clear
 174 upper hybrid signature have been retained. Two consecutive spectra are separated by
 175 about 7 s for the low rate data. A relatively smooth density profile, similar for the wave
 176 and the LP data set, is seen when the spacecraft enters or leaves Titan’s induced mag-
 177 netosphere. As illustrated in Figure 1, between about 15:45 UT and 16:10 UT and em-
 178 phasizes a good level of confidence on the electron density measurements.

179 Figure 2-a presents the overall density map in Titan’s environment deduced from
 180 these combined data sets. This map corresponds to the mean values of the electron den-
 181 sity sampled up to the T82 flyby. The mean values have been calculated by binning the
 182 data on a spatial grid where the abscissa is aligned with the TIIS X-axis and the ordi-
 183 nate is defined by $\rho_{TIIS} = \sqrt{Y_{TIIS}^2 + Z_{TIIS}^2}$. Cylindrical symmetry with respect to the
 184 TIIS X-axis is therefore assumed. The bin size used is 0.155 R_T (400 km), where $R_T =$
 185 2575 km is the radius of the Titan. Figure 2-b shows the map of the standard deviation
 186 of the electron density and Figure 2-c illustrates the sampled regions with th number of
 187 bins covered in our study.

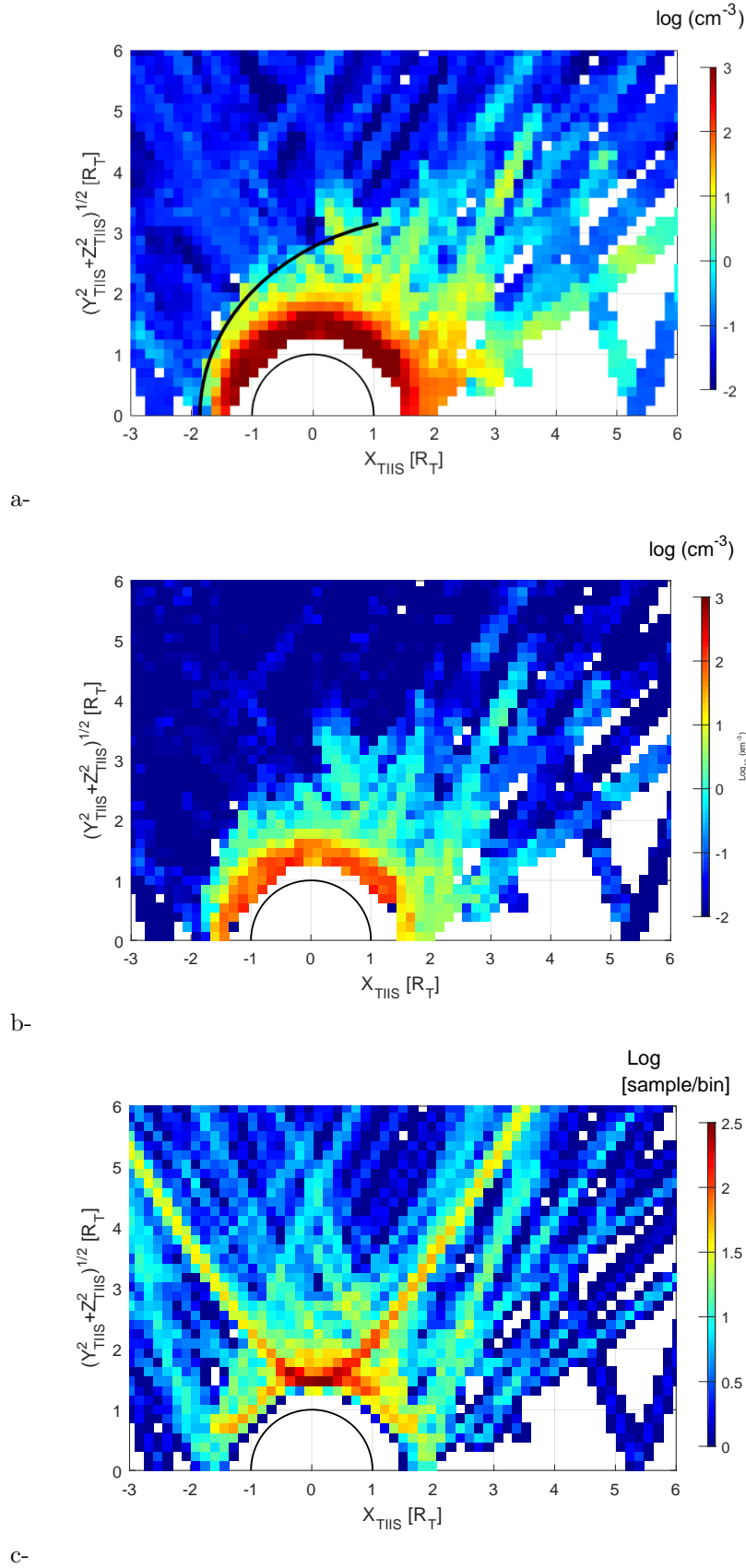


Figure 2. a- Global electron density map in a cylindrical frame centered on Titan deduced from combined RPWS and ELS observations from TA to T82. The black elliptical line indicates the location of the induced magnetosphere (cf text) b- Standard deviation map of electron number density. c- Cassini coverage for the TA-T82 flybys

188 Figure 2 includes all analyzed flybys, regardless of the external conditions. There-
 189 fore the presented electron density map includes varioussolar illumination conditions, up-
 190 stream plasma flow (electron density distribution, density and possibly composition), mag-
 191 netic field orientation (dipolar, planetward or swept-back fields). These different upstream
 192 conditions have been emphasized by Bertucci et al. (2009); Garnier et al. (2010); Rymer
 193 et al. (2009); Simon et al. (2010); Németh et al. (2011); Edberg et al. (2013); Regoli et
 194 al. (2018). Edberg et al. (2015) have carefully addressed the influence of Saturn’s mag-
 195 netosphere on Titan’s ionosphere, they also have shown that the dayside ionosphere is
 196 significantly denser than the nightside. Variation in these parameters affect Titan’s in-
 197 duced magnetosphere and contribute to blur the electron number density map. The re-
 198 sulting variability of the electron density is reflected in the standard deviation map (Fig-
 199 ure 2-b). The bin size, 400 km, might also contribute to increase the standard deviation
 200 value inside the density map bin since its spatial size is larger than the ionospheric scale
 201 height. Based on these maps, the characteristics of the plasma in the Titan environment
 202 can be summarized as follows. Firstly we observe a good statistical sampling of the iono-
 203 spheric region. Globally, a reasonable sampling was achieved for the induced magneto-
 204 sphere with more than 10 samples (from several flybys) in each bin with no statistical
 205 bias in the electron density map. Figure 2-a reveals a dense ionospheric region, with val-
 206 ues larger than $1000 \text{ electron cm}^{-3}$, with a relatively large standard deviation of several
 207 hundreds of electron cm^{-3} (Figure 2-b). This result is consistent with previous studies
 208 (e.g., Ågren et al., 2009; Edberg et al., 2010). The induced magnetosphere boundary sep-
 209 arates Saturn’s magnetospheric plasma from Titan’s ionospheric plasma. As seen in fig-
 210 ure 1, a sharp change on the density profile is usually observed. The induced magneto-
 211 sphere can be roughly identified at locations where the electron number density is larger
 212 than 1 cm^{-3} , since Saturn’s magnetospheric plasma do not reach such density value at
 213 Titan’s orbit (?). Similar location of Titan’s induced magnetospheric boundary can
 214 be derived from the gradient of the density profiles. A more accurate location of the in-
 215 duced magnetosphere might require to include criteria on the magnetic field and plasma
 216 flow observations.

217 In order to delimit the external envelop of the induced magnetosphere, we have fit-
 218 ted in the ram side and the near wake region, up to $X_{TIS} = 1 R_T$, the 1 cm^{-3} iso-
 219 contour with a function corresponding to an ellipse. Expressed in polar coordinates, as-
 220 suming a symmetry along the X_{TIS} axis, the equation of the induced magnetosphere

221 surface is $r = \frac{L}{1+\epsilon \cos \theta}$ where the polar coordinate (r, θ) are measured about the focus
 222 X_0 , L is the semi-major axis and ϵ is the eccentricity. The fitted conic parameters are
 223 $X_0 = 0.25 R_T$, $L = 2.52 R_T$ and $\epsilon = 0.57$. We did not extend the fit calculation in
 224 the middle and far Titan's wake because of the limited coverage. The fit of the induced
 225 magnetosphere boundary is represented by the black curve in figure 2-a. A conic func-
 226 tion has also been used to delimit the induced magnetosphere or magnetic pile-up bound-
 227 ary for Mars and Venus (and references therein Bertucci et al., 2011). Chen and Simon
 228 (2020) have shown that the magnetic pile-up boundary present some asymmetry in the
 229 Saturn facing/ anti-facing side due to the gyromotion of the pickup ions, emphasizing
 230 the limitation of the cylindrical symmetry assumption. Such asymmetry in the direction
 231 of the motional electric field has been also observed for the Martian induced magneto-
 232 sphere (Halekas et al., 2017; Dubinin et al., 2019).

233 Although figure 2-a does not show plasma composition, it suggests than Titan's
 234 planetary plasma can reach several tens of cm^{-3} at about $3 R_T$ and several cm^{-3} at about
 235 $6 R_T$ in the tail region. The induced magnetospheric boundary is closer to the planet
 236 on the ram side than on the flank side and the plasma scale height is much larger in the
 237 wake than on the ram side. From the induced magnetosphere fit, two parameters have
 238 been determined: R_{SD} which is the ellipse stand-off distance along the X_{TIIS} axis and
 239 R_{TD} which is the ellipse stand-off distance along the ρ_{TIIS} axis. We found $R_{SD} = 1.85$
 240 R_T and $R_{TD} = 2.77 R_T$. Simulation results are also consistent with this global elec-
 241 tron density map (e.g., Ledvina et al., 2012; Ma et al., 2006; Modolo & Chanteur, 2008;
 242 Sillanpää et al., 2006; Simon et al., 2007; Snowden et al., 2007).

243 The lack of coverage in the center of the far tail ($R > 3R_T$ and $\rho < 1R_T$) and
 244 the use of a cylindrical representation, does not allow a clear distinction of the two iono-
 245 spheric separated tail structures identified in a few flybys (Coates et al., 2012). Never-
 246 theless such a graphic provides an upper limit of the cross-section tail area at different
 247 distances in the tail, assuming a cylindrical symmetry, which might be useful to com-
 248 pute the ionospheric loss rate. For instance Coates et al. (2012) assumed an area of πR_T^2
 249 to compute the escape rate, similar to Modolo et al. (2007). According to Figure 2-b,
 250 the area of this disk might have been underestimated. A more detailed determination
 251 of the plasma loss rate is beyond the scope of this paper. The reader is referred to Wahlund
 252 et al. (2005), Coates et al. (2007), Szego et al. (2007), Modolo et al. (2007), Sittler et al.

253 (2010), Edberg et al. (2011), Coates et al. (2012), Westlake et al. (2012) and Romanelli
 254 et al. (2014), for some case studies of plasma loss rates estimates.

255 **4 Pick-up ions observations**

256 Ions from a planetary origin can be produced upstream of the induced magneto-
 257 sphere. These ions, incorporated into the background plasma flow, are so-called pick-up
 258 ions. They are accelerated by the motional electric field $\vec{E} = -\vec{v} \times \vec{B}$, moving in a plane
 259 perpendicular to B . Theoretical investigations and global hybrid simulation modeling have
 260 emphasized the asymmetry between the $+\vec{E}$ and $-\vec{E}$ hemispheres for pickup ions (Hartle
 261 et al., 2006; Modolo & Chanteur, 2008). The large gyroradii of the pickup ions have been
 262 also suggested to cause an asymmetry between Titan’s Saturn facing and adverted hemi-
 263 spheres on the magnetic pile-up profiles (Chen & Simon, 2020). In addition, due to their
 264 large gyroradius compared to the neutral scale height, pickup ions appear as narrow beams
 265 in velocity space (Hartle et al., 2006; Hartle & Sittler, 2007; Hartle et al., 2011).

266 The detection and characterization of ion cyclotron waves is another approach to
 267 identify the presence of pickup ions, as has been done for Mars or Venus (e.g., Romanelli
 268 et al., 2013; Delva et al., 2012). While direct measurements have identified this popu-
 269 lation at Titan from the ion mass spectrometer data, ion cyclotron waves are rarely ob-
 270 served at Titan in magnetic field data (Russell et al., 2016). An explanation, Cowee et
 271 al. (2010) suggested that the growth time is too long compared to the convection time
 272 of background plasma through the interaction region so that the ion cyclotron waves have
 273 not enough time to grow to amplitudes that can be observed by the Cassini magnetome-
 274 ter. Therefore data from the ion mass spectrometer remain the only and most direct way
 275 to study the pick-up ion population in Titan’s vicinity.

276 Regoli et al. (2016) have performed a survey of pickup up ions and found their pres-
 277 ence in the anti-Saturn side which leads to conclude that CAPS-IMS have captured freshly
 278 produced pickup ions. In this paper, we go one step further by organizing the pick-up
 279 ion observations in a reference frame depending of the magnetic field and characteriz-
 280 ing their progressive acceleration.

281 4.1 Pickup ion identification through their energy signature

282 Pickup ions signatures were searched in the CAPS-IMS data over the full set of
 283 T0a-T82 flybys. As examples, we found such signature at the edge of Titan's induced
 284 magnetosphere in flybys TA, T06, T39 and T42. Other flybys exhibit similar signatures.
 285 Figure 3 displays their energy characteristics and their location in 4 sets (a,b,c,d) cor-
 286 responding to the four mentioned flybys, each with 2 panels. The bottom panels of each
 287 set show Cassini trajectories drawn in cylindrical TIIS coordinates, while top panel dis-
 288 plays the average flux measured by the 8 anodes of CAPS-IMS. Patchy and repetitive
 289 structures observed in the magnetospheric region are due to the actuator motion of the
 290 platform hosting the particle instruments.

291 We clearly see the progressive deceleration of the incoming plasma on the inbound
 292 and outbound legs of each of these flybys and the entry of Cassini into Titan's ionosphere
 293 as indicated by low energy signatures (<100 eV) and high particle counts. The narrow
 294 beam energy signatures, indicated by the black arrows, suggest that these features arise
 295 from the detection of pickup ions. For these specific observations, the angle between the
 296 background magnetic field and the bulk plasma flow ranges between 70° and 140° . The
 297 observed ion pickup energy is smaller than the theoretical expected maximum, given by
 298 $4m_{pi}/m_{am}E_{am}\sin^2\theta_{vB}$ where m_{pi}/m_{am} is the ratio between ion pickup mass and the
 299 ambient ion mass, E_{am} is the energy of the ambient plasma, and θ_{vB} is the angle be-
 300 tween the ambient plasma flow velocity and the background magnetic field direction.

301 The location of the observed events are reported on the Cassini trajectory with black
 302 circle symbols. These events occur in the external part of the induced magnetosphere,
 303 usually near one of its flank, or in the kronian plasma region. This finding is consistent
 304 with global simulation results which reported pickup ions with relatively high energy in
 305 the flank of the induced magnetosphere, and more precisely in the +E hemisphere ac-
 306 cording to simulation results and theoretical expectations (e.g., Modolo & Chanteur,
 307 2008, their Figure 7).

308 The narrow beam signature in energy and velocity space is illustrated in Figure
 309 4. It shows the angular distribution of the plasma between 01:12 and 01:14 SCET at the
 310 energy bin 25 ($E=788$ eV) for the T63 flyby, in the Saturn Solar Ecliptic (SSE) coordi-
 311 nate system (Figure 4-a). In this coordinate system the X_{SSE} points towards the Sun,
 312 the Z_{SSE} is perpendicular to ecliptic plane, in the northern celestial hemisphere, and the

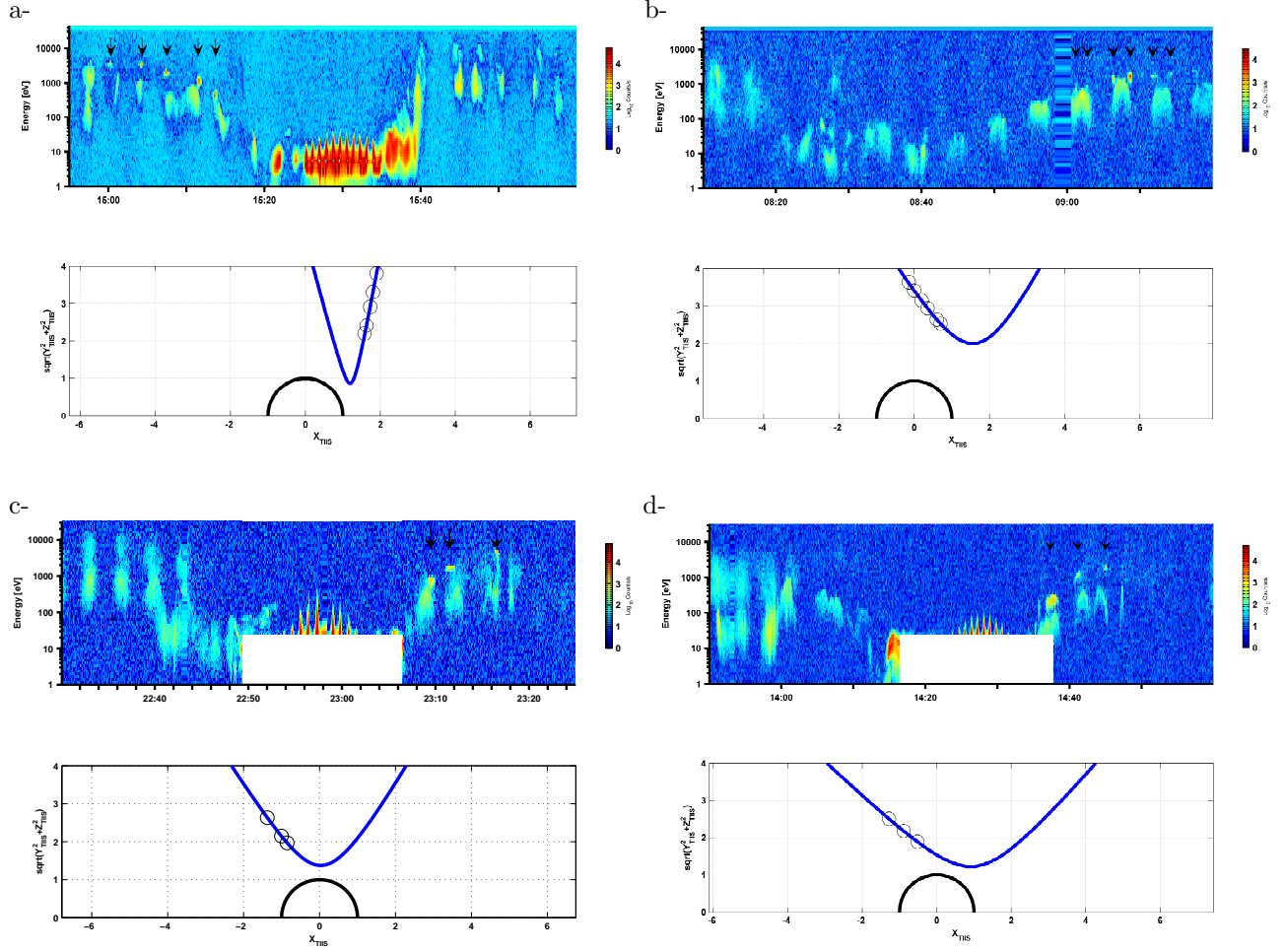


Figure 3. 4 set of figures (a,b,c,d) displaying the trajectory and CAPS-IMS observations for flybys TA, T06, T39 and T42, respectively. Each set has a top panel presenting CAPS-IMS observations and a bottom panel illustrating Cassini trajectory (blue line) for the corresponding flyby in cylindrical TIIS coordinate system. Black arrows in the CAPS-IMS panels indicate the presence of pickup ions. Their locations are reported on Cassini trajectory with a circle mark. The energy table change on CAPS-IMS near closest approach produces the white rectangles displayed on panels c and d.

313 Y_{SSE} completes the right hand system. The field of view of CAPS-IMS during this 2 min
 314 time interval covers only a small part of the full-sky. We can see an increase of counts/s
 315 in a very localized area pointing toward $-Y_{SSE}$, corresponding to the pickup ions. The
 316 instrument is therefore capturing ions moving away from Saturn, consistent with the ex-
 317 pected electric field direction and the cartoon of Titan's environment illustrated in Waite
 318 et al. (2004).

319 Figure 4-b displays, in polar (r, θ) coordinates, the energy-pitch angle distribution
 320 for the same time interval. The magnetic field measurements have been averaged dur-
 321 ing the 2 min interval. The r coordinate represents the energy in a logarithmic scale, from
 322 1 eV to 46 keV, while the θ coordinate indicates the pitch angle. The $\pm x$ direction of
 323 the plot implies a parallel / anti-parallel direction (with respect to the local magnetic
 324 field) and the y direction means a direction perpendicular to the magnetic field. Pickup
 325 ions are seen with a pitch angle close to 90° and with an energy slightly lower than 1 keV.
 326 Another example of energy - pitch angle and angular distribution is presented for the
 327 T70 flyby in Figure 4-c and d, and similar conclusions are reached.

328 4.2 Pickup ion mass composition

329 Hartle et al. (2006) reported on pickup ion composition for the TA flyby. TOF anal-
 330 ysis suggested the presence of H^+ , H_2^+ , N^+ / CH_2^+ , CH_4^+ and N_2^+ with possible contribu-
 331 tion of CH_3^+ , CH_5^+ , $HCNH^+$ and $C_2H_5^+$. The ion mass composition during flyby T39 (TOF
 332 acquisition from 23:11:48 to 23:16:04 SCET) indicates the presence of pickup ions reported
 333 next. Figure 5 displays the counts of the Straight Through (ST) detector as a function
 334 of energy per charge versus time of flight channel.

335 When ions enter through the CAPS-IMS sensor they first pass through the electro-
 336 static analyzer (ESA) which allow the determination of the energy per charge of the par-
 337 ticle. This information is presented on the y -axis of figure 5. At the exit of the ESA, par-
 338 ticles are pre-accelerated and impact a carbon foil, emitting secondary electrons. These
 339 electrons are attracted by the positive $\sim 15kV$ potential and hit the the ST detector
 340 giving the start signal of the TOF for the mass identification. When atomic or molec-
 341 ular species pass through the carbon foil they are break up in more elementary parti-
 342 cles (neutral particles, positively or negatively charged ions). Neutral atoms and nega-
 343 tively charged particles travel through the TOF chamber and hit the ST detector, pro-

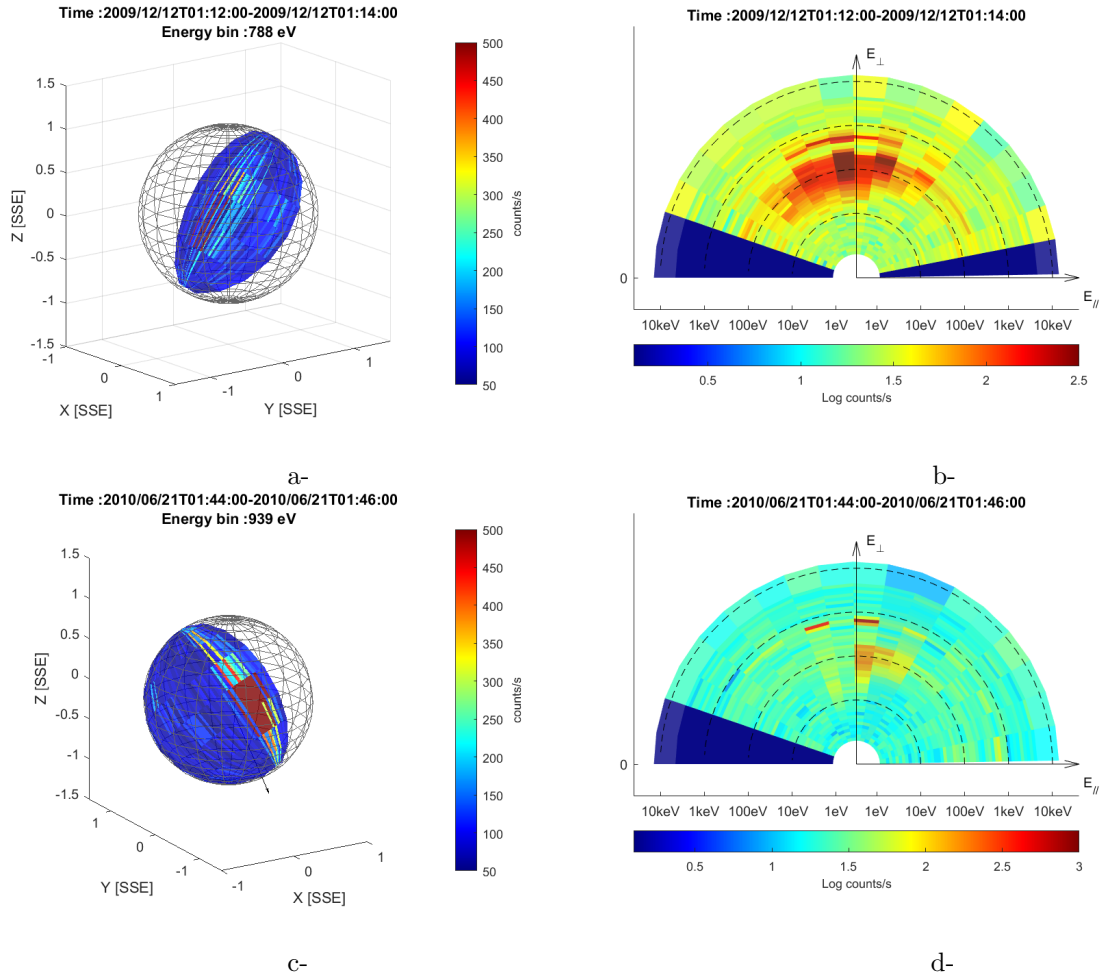


Figure 4. Panels a and c show the angular distribution during the T63 and T70 flyby respectively in the SSE coordinate system. Pickup ions have been indentified at time 01:12-01:14 SCET and at the energy 788 eV for the 63 flyby and at time 01:44-01:46 SCET at the energy 939 eV for the T70 flyby. Panel b and d display energy - pitch angle distribution in polar coordinate.

344 ducing a stop signal. The difference of time between the start and the stop signals de-
 345 termine the time of flight and is presented on the x -axis of figure 5. For a given energy
 346 per charge, lighter species will have shorter time of flight than heavier species and will
 347 be identified at smaller TOF channels. A more detailed description of the CAPS IMS
 348 instrument and the mass identification can be found in Young et al. (2004), Wilson et
 349 al. (2012) and Thomsen et al. (2014).

350 In this B-cycle (Figure 5) , the ion energies range from about 10 eV to few keV and
 351 there is a mixture of ambient and pick-up ions. Figure presents a mixture of ambient and
 352 pickup ions. Thomsen et al. (2010), and Wilson et al. (2017) have presented ion moments
 353 at Titan’s orbit indicating that H^+ , W^+ (water group ions) and H_2^+ compose to the mag-
 354 netospheric plasma. On the other hand, Felici et al. (2018) have suggested that Titan
 355 could also be a source of H_2^+ ions due to a maximum ratio of H_2^+/H^+ near Titan’s or-
 356 bit. For ions below 1 keV, the compositional analysis reveals H^+ and H_2^+ ions. The am-
 357 bient plasma differs from the pick-up ion population not only from their energy signa-
 358 ture but also from their incoming flow direction. The low energy species present a dif-
 359 ferent angular distribution compare to the 1 keV species, indicating different flow direc-
 360 tions and therefore suggesting distinct populations.

361 At about 1 keV, the spectrogram indicates heavier species. These ion species with
 362 an energy slightly above 1 keV correspond to the IMS energy pickup ion identification
 363 presented at Figure 3-c (first black arrow). By filtering TOF data in the energy range
 364 1-3 keV, one can thus determine the mass composition of the pick-up ion alone.

365 A simulation model, developed by Nelson and Berthelier (2009), characterizing the
 366 IMS instrumental response to various ion compositions at different energy, has been used
 367 to interpret the TOF signatures as accurately as possible. Simulation results have been
 368 compared to test chamber calibration measurements for several ion masses (atomic and
 369 molecular species with mass ranging from 12 to 28 amu) and at different energies (from
 370 1024 eV to 27560 eV). The simulation model is able to reproduce most of the observed
 371 IMS calibrated ST and LEF (Linear Electric Field) measurements for a specific ion species
 372 at a given energy.

373 A library of ST and LEF signatures for several atomic and molecular species with
 374 different energies has been built. By considering different compositions for this plasma
 375 we are able to compare the ion-summed simulated signatures with the measurements.

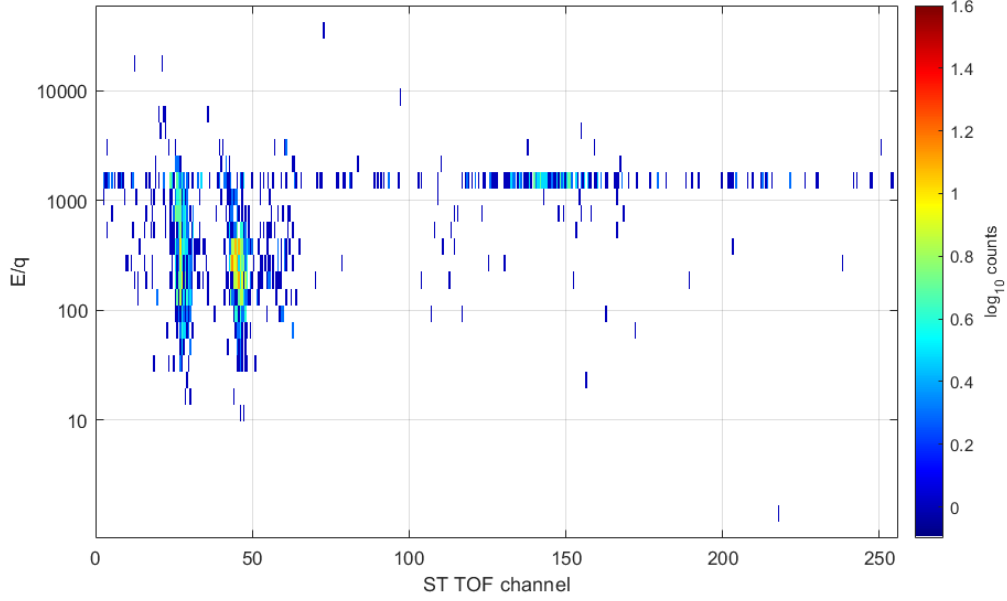


Figure 5. IMS-TOF spectrogram of the ST detector for the T39 flyby acquired at $\sim 23:11$ SCET. Counts, color coded with a logarithmic scale, on the ST detector are plotted as energy per charge (E/q [eV]) versus TOF channels.

376 Figure 6 top panel presents simulated results of several ion species at $\sim 1\text{keV}$ (H^+ , H_2^+ ,
 377 CH_3^+ , $HCNH^+$ and N_2^+). Figure 6 bottom panel displays a comparison between sim-
 378 ulated result and TOF observations. From the simulated results, three main patterns
 379 on the ST are expected for CH_3^+ (green curve) ions at 1keV , according to the simula-
 380 tion model. The main CH_3^+ peak located around TOF bin 150, contributing to the peak
 381 identified by label (2) in the bootom panel, is produced by a start signal issued by an
 382 electron and a stop signal from a neutral carbon atom. The second CH_3^+ peak at TOF
 383 bin 100 corresponds to the case of a start generated by an electron and stop generated
 384 by a negatively charged carbon ion C^- . A more diffuse contribution around TOF bin
 385 50, identified as the label (3) in the bottom panel, is believed to be due to a start time
 386 initiated by an electron and a stop time of a secondary electron ejected from high volt-
 387 age rings after an impact of neutral carbon or hydrogen atom. Each species has its own
 388 signature on the ST and LEF. As can be seen in Figure 6, it is impossible to dissociate
 389 the contribution from $HCNH^+$ (yellow) from N_2^+ (magenta) at this energy on the ST.
 390 The two curves are superimposed at TOF bins 190-240 and are expected to be due to
 391 a start/stop time infered by an electron and neutral nitrogen and carbon atoms, produc-

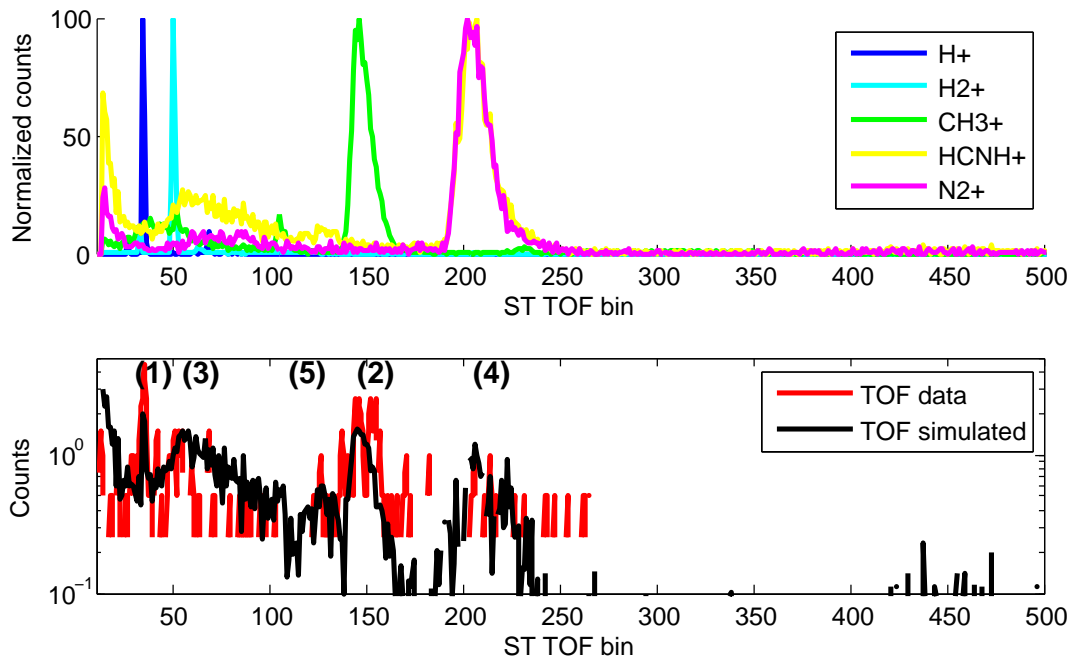


Figure 6. Simulated ST signatures for ion species at about 1keV (H^+ , H_2^+ , CH_3^+ , N_2^+ and $HCNH^+$) are presented on the top panel while the bottom panel displays a comparison between ST IMS-TOF counts and simulated results. ST observations have been acquired at $\sim 23:11$ SCET during the T39 flyby.

392 ing the relatively large peak label (4) in the simulation/observation comparison panel.
 393 Due to the small pick-up ion flux, no significant count rates on the LEF helps thus pre-
 394 venting to distinguish between these 2 different species. Peaks label (1) and (5) in the bot-
 395 tom panel correspond to a start/stop time due to an electron and a neutral hydrogen
 396 in the first case and an electron and c^- and N^- in the second case. The overall signa-
 397 tures thus indicate that the ion population near the flank of the induced magnetosphere
 398 is mainly composed of H^+ , CH_3^+ , $HCNH^+$ or N_2^+ . Thus, this pickup composition for
 399 flyby T39 is similar to the TA observations (Hartle et al., 2006).

400 Unfortunately TOF measurements by CAPS-IMS do not always allow determin-
 401 ing the mass composition due to insufficient number of counts on the LEF and ST de-
 402 tectors. Nevertheless, when available, TOF measurements present signatures similar to
 403 those shown in Figure 6 and suggesting the presence of the methane group (CH_2^+ , CH_3^+ ,
 404 CH_4^+ , CH_5^+) as well as of heavier species such as H_2CN^+ or N_2^+ . The column 7 of Ta-
 405 ble 1 summarizes the information on the mass composition of picku ions when a mass
 406 identifications of the pick-up ions was possible.

407 **4.3 Pickup location and energization**

408 The characteristicse of pickup ions are intrinsically related to the motional elec-
 409 tric field and magnetic field directions. Bertucci et al. (2009) and Simon et al. (2010) have
 410 shown that the magnetic field at Titan is highly variable and only few of the flybys gives
 411 an ambient field matching the Voyager 1 conditions. Therefore the geographical TIS
 412 coordinate system is not the most appropriate, and a draping coordinate system based
 413 on the incoming flow and magnetic field direction is expected to better describe, orga-
 414 nize and help in the interpretation of the formation of the induced magnetosphere. In
 415 this draping system, the X_{DRAP} axis is aligned with the corotational flow direction, the
 416 Z_{DRAP} axis points in the opposite direction of $\overrightarrow{B_{z_{DRAP}}} = \overrightarrow{B_{y_{TIS}}} + \overrightarrow{B_{z_{TIS}}}$ and Y_{DRAP}
 417 completes the right handed system. Such a coordinate system is similar to the DRAP
 418 system suggested by Neubauer et al. (2006), except that a non-zero $B_{x_{DRAP}}$ component
 419 is allowed, affecting the location of Titan's neutral sheet.

420 Bertucci et al. (2009) have shown that the Saturn magnetodisk strongly affects Ti-
 421 tan's upstream magnetic environment and exposes the moon to either dipolar-like fields
 422 close to SLT 12h and planetward, or sweptback fields in the midnight, dawn and dusk

423 sectors. To derive meaningful average ambient magnetic fields, it is important to infer
 424 time scales for Titan’s interaction. Based on one study by Bertucci et al. (2008), so called
 425 fossil magnetic field lines have been observed in Titan’s ionosphere. They provide infor-
 426 mation about the ”age” of draped magnetospheric field lines and their convection time
 427 in the ionosphere. Lifetimes of these field lines are expected to range between 20 min
 428 to 3 hours. This time interval corresponds to the time for a magnetospheric magnetic
 429 flux tube to reach Titan’s deep ionosphere (1000-1200 km altitude).

430 In our study the ambient magnetic field is averaged during a 30 min period inbound
 431 and a 30 min period outbound of each flyby. The time intervals used to compute the av-
 432 erage values have been taken such that the spacecraft is located outside of the region with
 433 draped field lines around Titan. Since our study focuses on the external part of the in-
 434 duced magnetosphere, short time intervals close to Titan’s induced magnetosphere are
 435 favored over larger intervals while the deep ionosphere will take a longer time to be af-
 436 fected by the upstream conditions. Magnetic field averages used for this study are, some-
 437 times, slightly different from those suggested by Simon et al. (2010) who averaged over
 438 longer time intervals (about 3 hours inbound and 3 hours outbound). Table 1 reports
 439 a synthesis of information on the flybys analyzed showing a signature of Titan’s induced
 440 magnetosphere. Each flyby is identified by its denomination, the date and time of its clos-
 441 est approach. The location of Titan with respect to Saturn is indicated in the Saturn
 442 Local Time (SLT) column and shows that all configurations are covered, although the
 443 pick-up ion region might not be explored for all local times. The average ambient mag-
 444 netic field inbound and outbound in the TIIS coordinate, as well as the presence of pick-
 445 up ion signatures determined from their energy characteristic and composition by CAPS/IMS
 446 are reported in the respective columns.

447 To compute the draped coordinate system, we assumed a linear dependance be-
 448 tween the inbound and outbound magnetic field values. The draped coordinate system
 449 is therefore computed for the time of each flyby and observations are represented in this
 450 changing reference frame. When the determination of an average ambient field (inbound
 451 or outbound) is impossible, either due to large variations in the kronian plasma or the
 452 difficulty to determine accurately when the spacecraft is located in kronian plasma re-
 453 gion, we assumed that the ambient field is constant during the whole flyby. In the cases
 454 where both inbound and outbound average magnetic field could not be determined, re-
 455 sults are displayed in the TIIS coordinate system.

456 Figure 7 shows a global overview of Titan’s induced magnetosphere. It represents
 457 the projection of Cassini trajectories in dashed lines in the YZ plane of the DRAP, or
 458 TIIS, coordinate system depending on the possibility to determine the average upstream
 459 magnetic field. Curved trajectories are due to the temporal changes of the draped ref-
 460 erence frame. In this coordinate system the upstream magnetic field direction points in
 461 the $-Z_{DRAP}$ direction while the convective electric field is directed along the $-Y_{DRAP}$
 462 axis.

463 The bi-polarity of Titan’s induced magnetosphere is emphasized with a clear re-
 464 veersal of the B_x component of the magnetic field indicating two magnetic lobe struc-
 465 tures formed by the interaction of the moon ionosphere and the kronian plasma. The
 466 local B_x component is plotted along the DRAP/TIIS trajectory where the electron den-
 467 sity is larger than 1 cm^{-3} . This result is compliant with the magnetotail structure char-
 468 acterized by Simon et al. (2010). Although the average magnetospheric field $\langle B_x \rangle$
 469 value has been subtracted in order to remove a possible displacement of the neutral sheet
 470 due to the respective location of Titan with respect to Saturn’s magnetodisk, the B_x re-
 471 veersal is not centered in the $Z = 0$ plane but may vary from flyby to flyby. It might
 472 be due to a North-South asymmetry of the magnetospheric flow or to a violation of the
 473 simplifying assumption that the magnetospheric field vary linearly between inbound and
 474 outbound magnetic field values, leading to an inaccurate estimate of the DRAP coor-
 475 dinate system.

476 Observed pick-up ion locations are displayed with filled circles (DRAP coordinate
 477 system) or squares (TIIS coordinate system) and the green-yellow color code indicates
 478 the energy. When the mass composition could be inferred, the symbol is surrounded by
 479 a red circle. All pick-up ions signatures found are localized in the $+E$ hemisphere, as ex-
 480 pected from test-particle and global simulations (e.g., Luhmann, 1996; Modolo & Chanteur,
 481 2008). Pickup ions with the lowest energy are observed preferentially in a range of Z_{DRAP}
 482 values between $\pm 2 R_T$. Pickup ions with or without their mass composition present sim-
 483 ilar characteristics in term of position and energy. A progressive energization is clearly
 484 demonstrated by these Figures since pick-up ions observed farther from Titna reach higher
 485 energies up to several keV. Pickup gyroradius for ions of $m/q = 16$ and 28 in a typi-
 486 cal kronian plasma at Titan’s orbit is $\sim 2 R_T$ and $\sim 3.5 R_T$, respectively. Comparing
 487 these gyroradii with the pickup location in Figure 7 we can conclude that CAPS cap-
 488 tured these pickup ions during their first gyration.

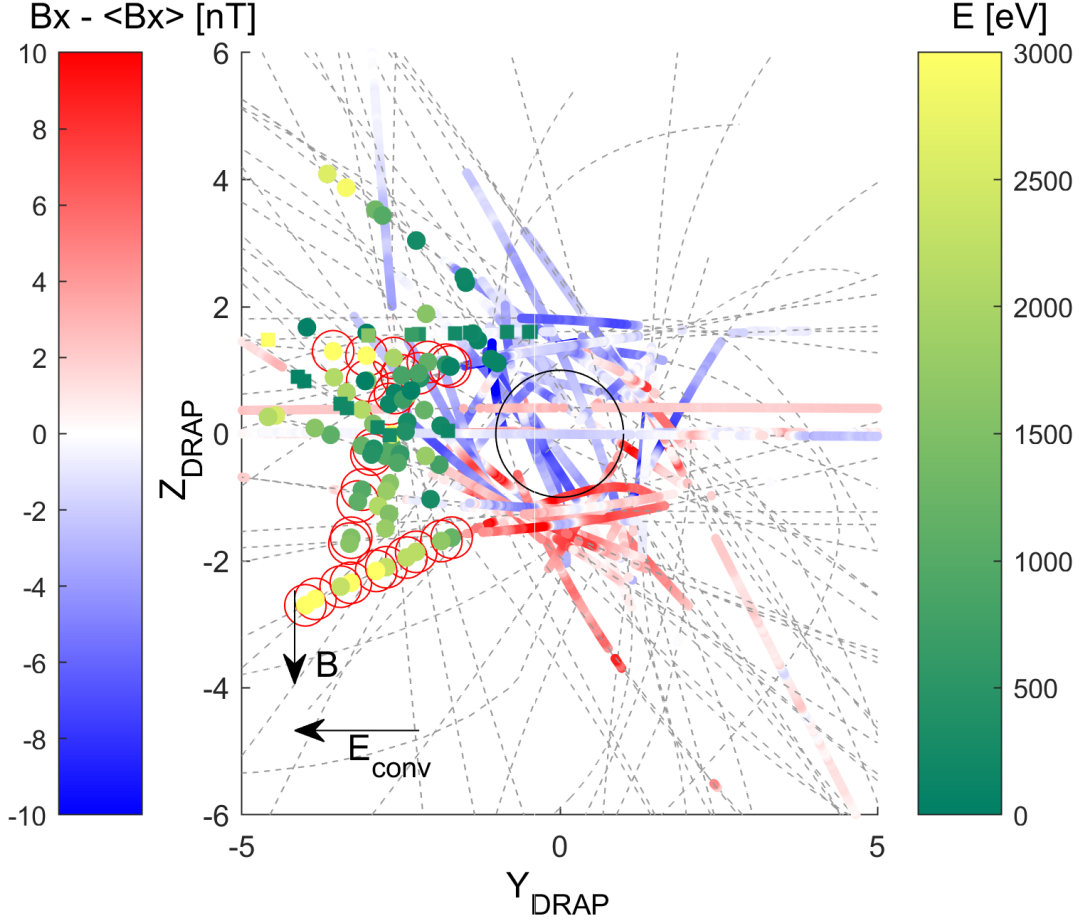


Figure 7. Projection of the Cassini flyby in the YZ_{DRAP} plane. Cassini's trajectories, in the DRAP coordinates, are shown by the dashed lines. Along the trajectory, the $B_x - \langle B_x \rangle_{upstream}$ are colored, in blue-red colorbar, only in the induced magnetosphere region ($n_e > 1cm^{-3}$) and it emphasizes the two magnetic lobe polarities due to the draping. Filled dots and square symbols represent the pickup location in the DRAP and in the TIIS coordinates (when the upstream magnetic field could not be computed). The color code green-yellow colorbar, represent the energy in eV of the pickup ions. Filled dots with a red circle indicate the pickup ion when the mass composition could be determined.

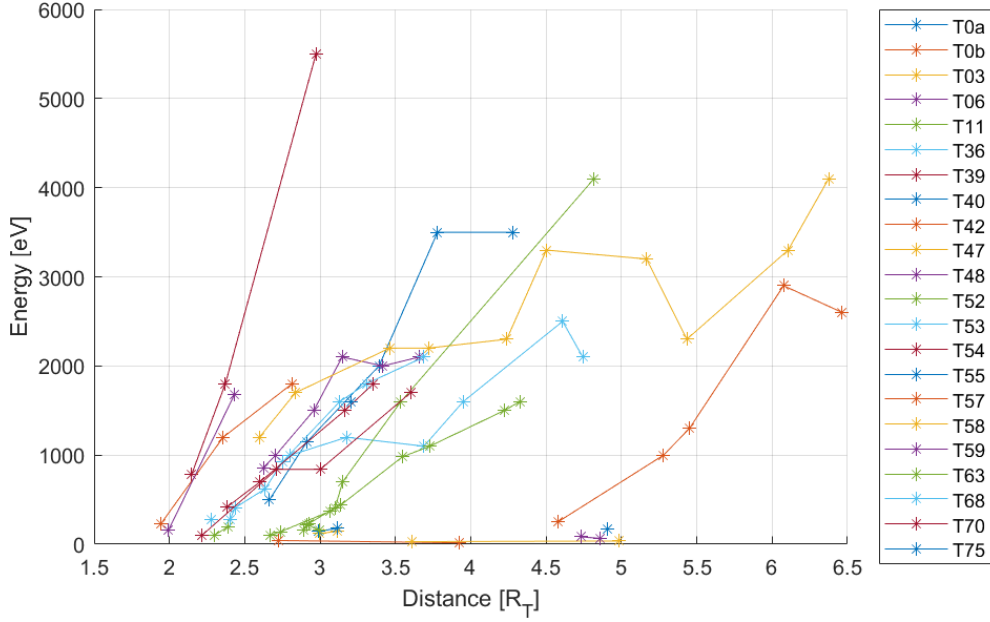


Figure 8. Pickup ion energy (in eV) in function of the distance to Titan (in R_T) for the different flybys where pickup ion have been identified.

489 Figure 8 displays the energy of the pickup ions as a function of the distance for fly-
 490 bys with pickup ion signatures. A clear linear relationship between the distance to the
 491 moon and the energy (up to 5.5 keV) is observed for a large majority of flybys. Assum-
 492 ing that the electric field is constant during a flyby outside of the induced magnetosphere,
 493 and integrating the equation of motion of a charged particle in a uniform electric field
 494 we can show that the energy gain of the particle depends on the electric field and the
 495 distance of acceleration ($\mathcal{E} = qE_{\perp}x$, with x the distance). A linear regression analy-
 496 sis for each flybys, having at least three pickup ion energy signatures, therefore provides
 497 an estimate of the intensity of the perpendicular component of the kronian electric field.
 498 We found that the kronian electric field varies between 0.22 mV/m and 2.24 mV/m, de-
 499 pending of the flybys. Averaging over all selected flybys, the kronian electric field is $E_{\perp} \simeq$
 500 0.70 mV/m. According to Wilson et al. (2017) the plasma velocity at 20 Saturn radii
 501 varies between ~ 50 km/s and ~ 200 km/s. The background magnetic field at Titan's
 502 orbit ranges from ~ 2 nT to ~ 6.5 nT with an average value of 4.4 nT, estimated from
 503 Table 1. With a typical velocity of 140 km/s along the corotation direction and an av-
 504 erage magnetic field of 4.4 nT aligned with the Z_{TIIIS} axis, the electric field is $E_{theo} =$

505 $|\vec{v} \times \vec{B}| \simeq 0.61$ mV/m in very good agreement with the electric field intensity estimate
 506 derived from pick-up ions.

507 **5 Conclusions**

508 Magnetometer data from MAG, particle data from CAPS and waves observations
 509 from RPWS have been combined to present a global picture of Titan's induced magne-
 510 tosphere and its pickup ion population.

511 Data from the CAPS-ELS electron spectrometer together with plasma wave ob-
 512 servations from RPWS have provided for the whole set of flybys, from T0a to T82, con-
 513 tinuous electron density profile ranging from 10^{-2} to several 10^3 ions. cm^{-3} . These pro-
 514 files have been used to infer a global electron density map of Titan's near environment.

515 The cold ionspheric plasma is confined on the ram-side below $\sim 1.85 R_T$ to ~ 2.77
 516 R_T , while it has been observed to extend farther than 6 Titan radii in the wake region.
 517 The denser part of the induced magnetosphere is located in the ionosphere as expected,
 518 while an extended plasma wake is reported. Although other factors, such as plasma beta,
 519 local time and seasonal effects are expected to affect Titan's ionized environment, the
 520 draping coordinate system proposed in this paper emphasizes the organization of Titan's
 521 induced magnetosphere with respect to the kronian magnetic field. In the plane perpen-
 522 dicular to the ideal corotational flow, an elliptical envelope elongated along the ambi-
 523 ent field direction contains the cold plasma, supported by a clear evidence of bipolar mag-
 524 netotail geometry. It can be used to determine an upper limit of a cross-section tail area,
 525 required to compute total plasma loss rates.

526 Upstream of the induced magnetosphere, detection of pickup ions have been ob-
 527 served and characterized with the ion mass spectrometer onboard Cassini spacecraft. The
 528 mass composition of these pickups ions was determined in a few cases and time of flight
 529 measurements have indicated the presence of methane group ions, molecular nitrogen
 530 or $HCNH^+$ ions and lighter species such as protons and molecular hydrogen ions. These
 531 pickup ions have been reported on the $+E$ hemisphere, close to the magnetic equator,
 532 supporting theoretical or modelling results. A progressive energization is also observed,
 533 and pickup ions with few keV have been identified as close as ~ 2 Titan radii. From their
 534 energy signatures, the background electric field intensity is retrieved. Its value varies be-
 535 tween 0.22 mV/m and 2.24 mV/m, with an average value of $\simeq 0.70$ mV/m in agreement

536 with a typical electric field assuming a plasma flow of 140 km/s and a magnetic field of
537 4.4 nT reported by recent studies.

Table 1: Titan flyby information. The first column indicates the reference number, the time of the closest approach and the Saturn location are reported in the second and third columns. The average background magnetic field, inbound and outbound are presented in the fourth and fifth column while the last two columns mark the presence of pickup ions by their energy signature and their mass composition respectively.

Flyby	Time (CA)	SLT [h]	B_{TIIS} [nT] Inbound	B_{TIIS} [nT] Outbound	Pick-up (Energy signature)	Pick-up (ion mass composition)
TA	2004-10-26T15:30:00.0	10.6	(0.4,2.6,-6.1)	(0.5, 2.7, -4.6)	x	N^+ / CH_2^+ , CH_4^+ , $HCNH^+$ Hartle et al. (2006)
TB	2004-12-13T11:27:29.0	10.5	(0.9,3.8,-3.2)	(0.5,2.7,-4.6)	x	-
T03	2005-02-15T06:54:21.0	10.3	(1.4,3.6,-4.2)	(1.8,3.7,-4.00)	x	-
T05	2005-04-16T19:05:57.0	5.3	(1.7, 6.2, -4.7)	(2.4, 5.2, -4.1)		
T06	2005-08-22T18:54:50.0	5.0	(1.5,2.4,-1.1)	(0.3,3.5,-2.3)	x	-
T08	2005-10-28T03:58:09.0	9.3	(1.4,3.1,-2.4)	(1.9,4.1,-1.8)	-	-
T10	2006-01-15T11:36:46.0	8.5	(2.6,3.7,-3.5)	(3.0,3.6,-3.1)	-	-

T11	2006-02-27T08:20:44.0	1.1	(1.4,2.5,-2.9)	(0.1,3.9,-2.6)	x	-
T12	2006-03-12T23:58:17.0	6.4	(1.7,5.0,-2.9)	(3.3,5.6,-2.5)	-	-
T13	2006-04-30T20:53:31.0	23.2	(1.81,1.28,0.97)	(0.69,2.66,-2.46)	-	-
T14	2006-05-20T12:13:05.0	4.4	(0.9,4.4,-2.1)	(2.2,4.8,-2.1)	-	-
T15	2006-07-02T09:12:19.0	21.2	(2.1,3.6,-1.4)	(0.8,3.8,-2.3)	-	-
T16	2006-07-21T00:25:13.0	2.4	(-0.1,-1.5,-3.4)	(1.7,1.0,-2.4)	-	-
T17	2006-09-07T20:12:04	2.3	(0.0,2.8,-2.3)	(2.2,4.0,-1.4)	-	-
T18	2006-09-23T18:52:44.0	2.3	(1.8,5.0,-0.8)	(2.2,4.6,-1.1)	-	-
T19	2006-10-09T17:23:24.0	2.2	(-4.2,1.7,4.0)	(-0.6,2.6,-6.0)	-	-
T20	2006-10-25T15:51:29.0	2.2	(2.2,4.6,0.5)	(3.6,5.1,-0.4)	-	-
T21	2006-12-12T11:35:17.0	2.1	(3.3, 4.8, -1.4)	(2.8, 5.4, -1.2)	-	-
T22	2006-12-28T10:00:13.0	1.9	(2.1, 4.3, -1.7)	(0.6, 3.7, -2.1)	-	-
T23	2007-01-13T08:34:00.0	2.0	(3.0,5.3, -0.9)	-	-	-
T24	2007-01-29T07:12:10.0	1.9	(2.2, 4.4, -0.7)	(2.6, 4.7, -0.8)	-	-
T25	2007-02-22T03:10:59.0	13.9	(0.2, -0.2, -2.8)	-	-	-
T26	2007-03-10T01:47:22	13.8	(2.3, 1.8, -2.7)	(0.8, 2.9, -2.5)	-	-
T27	2007-03-25T00:21:52.0	13.8	(0.6, 1.2, -2.0)	(-0.4, 0.6, -2.7)	-	-
T28	2007-04-10T22:57:11.0	13.7	(-0.8, 0.0, -6.2)	(0.8, 1.5, -5.2)	-	-

T29	2007-04-26T21:32:52.0	13.7	(-0.4, 1.8, -3.9)	(-1.9, 2.4, -6.4)	-	-
T30	2007-02-12T20:08:14.0	13.6	(-0.4, 2.3, -4.1)	(-2.1, 0.3, -4.0)	-	-
T31	2007-05-28T18:51:27.0	13.6	(0.3, 1.5, -3.5)	-	-	-
T33	2007-06-29T17:05:01.0	13.6	(-1.9, 2.2, -4.2)	(-0.9, 3.4, -5.3)	-	-
T34	2007-07-18T00:41:02.0	18.8	(-1.6, 2.3, -1.8)	(0.4, 2.1, -2.5)	-	-
T35	2007-08-31T06:34:25.0	11.5	(1.0, 3.0, -1.2)	-	-	-
T36	2007-10-02T04:49:50.0	11.5	(2.3, 1.9, -5.3)	(1.3, 0.7, -3.3)	x	CH_2^+ , CH_3^+ , CH_4^+ , H_2CN^+ , H^+ , H_2^+
T37	2007-11-19T00:52:51.0	11.4	(0.7, 2.3, -1.6)	-	-	-
T38	2007-12-04T00:07:37.0	11.4	(3.0, 1.8, -4.4)	(1.1, 0.8, -6.0)	-	-
T39	2007-12-20T22:56:41.0	11.4	(-0.2, 1.1, -9.1)	-	x	-
T40	2008-01-05T21:26:24.0	11.3	(-0.5, 2.0, -1.9)	-	x	-
T41	2008-02-22T17:39:23.0	11.2	(1.2, 3.5, -2.5)	-	-	-
T42	2008-03-25T14:36:12.0	11.1	(-0.4, 0.7, -8.0)	-	-	-
T43	2008-05-12T10:09:59.0	11.0	(0.6, 0.4, -4.0)	(-0.3, 2.7, -3.4)	-	-
T44	2008-05-28T08:33:21.0	10.9	(0.3, 0.4, -5.5)	(-0.6, 0.5, -7.2)	-	-
T45	2008-07-31T02:13:11.0	10.7	(1.6, 3.3, -2.1)	-	-	-
T46	2008-11-03T17:35:23.0	10.5	(1.8, 2.0, -0.7)	(-0.1, 1.6, -1.2)	-	-
T47	2008-11-19T15:56:28.0	10.4	(0.9, 0.7, -1.6)	(-0.4, -1.0, -1.6)	x	CH_2^+ , CH_3^+ , CH_4^+ , H^+ , H_2^+

T48	2008-12-05T14:25:45	10.4	(1.3, 2.8, -1.3)	(-0.4, 1.0, -1.5)	x	-
T49	2008-12-21T12:59:53	10.3	(2.3, 3.8, -3.1)	(0.7, 3.2, -2.7)	-	-
T50	2008-02-07T08:50:51	10.2	(2.9, -0.2, -1.7)	(0.9, 0.3, -2.7)	-	-
T51	2009-03-27T04:43:36	10.1	(1.2, 3.1, -1.4)	(0.5, 0.3, -3.8)	-	-
T52	2009-04-04T01:47:47	22.1	(1.3, 3.1, -1.4)	(0.5, 0.4, -3.9)	x	CH_3^+ , CH_4^+ , H_2CN^+ , N_2^+ , H_2^+ , H^+
T53	2009-04-20T00:20:45	22.1	(0.2, -0.3, -3.2)	(1.5, 1.7, -2.4)	x	
T54	2009-05-05T18:32:35	22.0	(1.9, 4.3, -0.9)	(-1.5, -2.2, -0.9)	-	
T55	2009-05-21T21:26:41	22.0	(0.1, 1.4, -0.9)	(1.3, 3.6, -1.4)	x	-
T56	2009-06-06T20:00:00	21.9	(0.7, 5.4, -1.7)	(-2.9, -1.3, -1.5)	-	-
T57	2009-06-22T18:32:35	21.9	(0.9, 0.8, -2.3)	(2.5, 4.0, -1.6)	x	-
T58	2009-07-08T17:05:009	21.8	(2.0, 4.1, 0.5)	(-0.3, 2.0, -1.8)	x	-
T59	2009-07-24T15:35:09	21.8	-	-	x (TIIS)	CH_3^+ , CH_4^+ , CH_5^+ , H_2CN^+ , H_2^+ , H^+
T61	2009-08-25T12:52:44	21.7	-	-	-	-
T62	2009-10-12T08:37:30	21.6	-	-	-	-
T63	2009-12-12T01:04:20	17.0	-	-	x (TIIS)	-
T64	2009-12-28T00:18:05	16.8	(-1.7, -1.5, -1.5)	(-0.9, -1.9, -1.7)	-	-
T65	2010-01-12T23:11:42	16.9	(0.2, 3.0, -4.8)	(-0.6, -2.5, -1.6)	-	-
T66	2010-01-28T22:29:55	21.0	-	-	-	-

T67	2010-04-05T15:51:44	16.1	-	-	-	-
T68	2010-05-20T03:25:26	16.0	(1.5, 1.9, -1.8)	(-1.1, -1.7, -1.5)	x	-
T69	2010-06-05T02:27:33	16.0	(0.5, -1.2, -3.3)	(1.5, 1.8, -2.6)	-	-
T70	2010-06-21T01:28:23	16.1	(0.1, -0.8, -4.6)	(0.1, -0.1, -5.9)	x	CH_4^+ , CH_3^+ , H_2CN^+ , H^+ , H_2^+ , CH_5^+ , H_2O^+
T71	2010-07-07T00:22:35	16.1	(0.3, -0.5, -2.7)	(0.7, 0.4, -2.7)	-	-
T72	2010-09-24T18:38:41	15.9	-	-	-	-
T74	2011-02-08T16:04:11	20.6	-	-	-	-
T75	2011-04-19T05:00:39	14.2	-	-	x (THIS)	-
T76	2011-05-08T22:53:44	19.8	-	-	-	-
T77	2011-06-20T18:32:01	12.2	(0.3, -1.4, -4.3)	(0.0, -1.4, -5.1)	-	-
T78	2011-09-12T02:50:05	17.5	(0.3, 1.9, -2.7)	(-1.8, -2.3, -2.2)	-	-
T82	2012-02-19T08:43:17	18.3	-	-	-	-

538 **Acknowledgments**

539 RM, JJB, PC, RP and FL are indebted to the "Soleil, Heliosphere, Magnetosphere" group
 540 of CNES for its support. It is based on observations with RPWS, CAPS, MAG embarked
 541 on Cassini. The Cassini data used in this paper are available at the NASA Planetary
 542 Data System (<https://pds-ppi.igpp.ucla.edu>). The authors are grateful to the French
 543 "Centre de Données sur la Physique des Plasmas" for the access to the visualization tools
 544 AMDA.

545 **References**

- 546 Ågren, K., Wahlund, J., Garnier, P., Modolo, R., Cui, J., Galand, M., & Müller-
 547 Wodarg, I. (2009, December). On the ionospheric structure of Titan. *Planet.*
 548 *Space Sci.*, *57*, 1821-1827. doi: 10.1016/j.pss.2009.04.012
- 549 Arridge, C. S. (2012). A statistical analysis of plasma parameters near Titan's orbit.
 550 *J. Geophys. Res.*
- 551 Arridge, C. S., Achilleos, N., & Guio, P. (2011, July). Electric field variability and
 552 classifications of Titan's magnetoplasma environment. *Annales Geophysicae*,
 553 *29*, 1253-1258. doi: 10.5194/angeo-29-1253-2011
- 554 Arridge, C. S., André, N., Bertucci, C. L., Garnier, P., Jackman, C. M., Németh,
 555 Z., ... Crary, F. J. (2011, December). Upstream of Saturn and Titan. , *162*,
 556 25-83. doi: 10.1007/s11214-011-9849-x
- 557 Arridge, C. S., André, N., McAndrews, H. J., Bunce, E. J., Burger, M. H., Hansen,
 558 K. C., ... Dougherty, M. K. (2011, December). Mapping Magnetospheric
 559 Equatorial Regions at Saturn from Cassini Prime Mission Observations. , *164*,
 560 1-83. doi: 10.1007/s11214-011-9850-4
- 561 Barabash, S. (2012, February). Classes of the solar wind interactions in the solar
 562 system. *Earth, Planets, and Space*, *64*(2), 57-59. doi: 10.5047/eps.2012.01
 563 .005
- 564 Bertucci, C., Achilleos, N., Dougherty, M. K., Modolo, R., Coates, A. J., Szego, K.,
 565 ... Young, D. T. (2008, September). The Magnetic Memory of Titan's Ionized
 566 Atmosphere. *Science*, *321*, 1475-. doi: 10.1126/science.1159780
- 567 Bertucci, C., Duru, F., Edberg, N., Fraenz, M., Martinecz, C., Szego, K., & Vais-
 568 berg, O. (2011, December). The Induced Magnetospheres of Mars, Venus, and
 569 Titan. , *162*(1-4), 113-171. doi: 10.1007/s11214-011-9845-1

- 570 Bertucci, C., Sinclair, B., Achilleos, N., Hunt, P., Dougherty, M. K., & Arridge,
 571 C. S. (2009, December). The variability of Titan's magnetic environment.
 572 *Planet. Space Sci.*, *57*, 1813-1820. doi: 10.1016/j.pss.2009.02.009
- 573 Chen, C., & Simon, S. (2020). A comprehensive study of titan's magnetic pile-
 574 up region during the cassini era. *Planetary and Space Science*, *191*, 105037.
 575 Retrieved from [http://www.sciencedirect.com/science/article/pii/](http://www.sciencedirect.com/science/article/pii/S0032063319305392)
 576 [S0032063319305392](http://www.sciencedirect.com/science/article/pii/S0032063319305392) doi: <https://doi.org/10.1016/j.pss.2020.105037>
- 577 Coates, A. J. (2009, February). Interaction of Titan's ionosphere with Saturn's mag-
 578 netosphere. *Royal Society of London Philosophical Transactions Series A*, *367*,
 579 773-788. doi: 10.1098/rsta.2008.0248
- 580 Coates, A. J., Crary, F. J., Young, D. T., Szego, K., Arridge, C. S., Bebesi, Z.,
 581 ... Hill, T. W. (2007). Ionospheric electrons in titan's tail: Plasma struc-
 582 ture during the cassini t9 encounter. *Geophysical Research Letters*, *34*(24).
 583 Retrieved from [https://agupubs.onlinelibrary.wiley.com/doi/abs/](https://agupubs.onlinelibrary.wiley.com/doi/abs/10.1029/2007GL030919)
 584 [10.1029/2007GL030919](https://agupubs.onlinelibrary.wiley.com/doi/abs/10.1029/2007GL030919) doi: 10.1029/2007GL030919
- 585 Coates, A. J., Johnstone, A. D., Huddleston, D. E., Wilken, B., Jockers, K., Borg,
 586 H., ... Neubauer, F. M. (1993, March). Pickup water group ions at Comet
 587 Grigg-Skjellerup. *Geophys. Res. Lett.*, *20*, 483-486. doi: 10.1029/93GL00174
- 588 Coates, A. J., Johnstone, A. D., Wilken, B., Jockers, K., & Glassmeier, K.-
 589 H. (1989, August). Velocity space diffusion of pickup ions from the
 590 water group at Comet Halley. *J. Geophys. Res.*, *94*, 9983-9993. doi:
 591 [10.1029/JA094iA08p09983](https://doi.org/10.1029/JA094iA08p09983)
- 592 Coates, A. J., Wellbrock, A., Lewis, G. R., Arridge, C. S., Crary, F. J., Young,
 593 D. T., ... Jones, G. H. (2012). Cassini in titan's tail: Caps observations of
 594 plasma escape. *Journal of Geophysical Research: Space Physics*, *117*(A5).
 595 Retrieved from [https://agupubs.onlinelibrary.wiley.com/doi/abs/](https://agupubs.onlinelibrary.wiley.com/doi/abs/10.1029/2012JA017595)
 596 [10.1029/2012JA017595](https://agupubs.onlinelibrary.wiley.com/doi/abs/10.1029/2012JA017595) doi: 10.1029/2012JA017595
- 597 Cowee, M. M., Gary, S. P., Wei, H. Y., Tokar, R. L., & Russell, C. T. (2010). An ex-
 598 planation for the lack of ion cyclotron wave generation by pickup ions at titan:
 599 1-d hybrid simulation results. *Journal of Geophysical Research: Space Physics*,
 600 *115*(A10). Retrieved from [https://agupubs.onlinelibrary.wiley.com/](https://agupubs.onlinelibrary.wiley.com/doi/abs/10.1029/2010JA015769)
 601 [doi/abs/10.1029/2010JA015769](https://agupubs.onlinelibrary.wiley.com/doi/abs/10.1029/2010JA015769) doi: 10.1029/2010JA015769
- 602 Cravens, T. E., Yelle, R. V., Wahlund, J.-E., Shemansky, D. E., & Nagy, A. F.

- 603 (2010). Composition and Structure of the Ionosphere and Thermosphere. In
 604 R. H. Brown, J.-P. Lebreton, & J. H. Waite (Eds.), *Titan from cassini-huygens*
 605 (p. 259). doi: 10.1007/978-1-4020-9215-2-11
- 606 Delva, M., Mazelle, C., & Bertucci, C. (2012). Upstream Ion Cyclotron Waves at
 607 Venus and Mars. In *The plasma environment of venus* (Vol. 37, p. 5). doi: 10
 608 .1007/s11214-011-9828-2
- 609 Dougherty, M. K., Kellock, S., Southwood, D. J., Balogh, A., Smith, E. J., Tsu-
 610 rutani, B. T., ... Cowley, S. W. H. (2004, September). The Cassini
 611 Magnetic Field Investigation. *Space Science Reviews*, 114, 331-383. doi:
 612 10.1007/s11214-004-1432-2
- 613 Dubinin, E., Fraenz, M., Woch, J., Barabash, S., Lundin, R., & Yamauchi, M.
 614 (2006, November). Hydrogen exosphere at Mars: Pickup protons and
 615 their acceleration at the bow shock. *Geophys. Res. Lett.*, 33, 22103. doi:
 616 10.1029/2006GL027799
- 617 Dubinin, E., Lundin, R., Koskinen, H., & Norberg, O. (1993, April). Cold ions at
 618 the Martian bow shock - PHOBOS observations. *J. Geophys. Res.*, 98, 5617-
 619 5623. doi: 10.1029/92JA02374
- 620 Dubinin, E., Modolo, R., Fraenz, M., Päetzold, M., Woch, J., Chai, L., ... Zelenyi,
 621 L. (2019). The induced magnetosphere of mars: Asymmetrical topology of
 622 the magnetic field lines. *Geophysical Research Letters*, 46(22), 12722-12730.
 623 Retrieved from [https://agupubs.onlinelibrary.wiley.com/doi/abs/](https://agupubs.onlinelibrary.wiley.com/doi/abs/10.1029/2019GL084387)
 624 10.1029/2019GL084387 doi: 10.1029/2019GL084387
- 625 Edberg, N., Ågren, K., Wahlund, J.-E., Morooka, M., Andrews, D., Cowley, S., ...
 626 Dougherty, M. (2011). Structured ionospheric outflow during the cassini
 627 t55-t59 titan flybys. *Planetary and Space Science*, 59(8), 788 - 797. Re-
 628 trieved from [http://www.sciencedirect.com/science/article/pii/](http://www.sciencedirect.com/science/article/pii/S0032063311000948)
 629 S0032063311000948 doi: <https://doi.org/10.1016/j.pss.2011.03.007>
- 630 Edberg, N. J. T., Andrews, D. J., Bertucci, C., Gurnett, D. A., Holmberg, M. K. G.,
 631 Jackman, C. M., ... Wahlund, J.-E. (2015). Effects of saturn's mag-
 632 netospheric dynamics on titan's ionosphere. *Journal of Geophysical Re-*
 633 *search: Space Physics*, 120(10), 8884-8898. Retrieved from [https://](https://agupubs.onlinelibrary.wiley.com/doi/abs/10.1002/2015JA021373)
 634 agupubs.onlinelibrary.wiley.com/doi/abs/10.1002/2015JA021373 doi:
 635 10.1002/2015JA021373

- 636 Edberg, N. J. T., Andrews, D. J., Shebanits, O., Ågren, K., Wahlund, J.,
 637 Opgenoorth, H. J., ... Girazian, Z. (2013). Solar cycle modulation of ti-
 638 tan's ionosphere. *Journal of Geophysical Research: Space Physics*, *118*(8),
 639 5255-5264. Retrieved from <https://agupubs.onlinelibrary.wiley.com/doi/abs/10.1002/jgra.50463> doi: 10.1002/jgra.50463
- 641 Edberg, N. J. T., Wahlund, J.-E., Ågren, K., Morooka, M. W., Modolo, R., Bertucci,
 642 C., & Dougherty, M. K. (2010, October). Electron density and temperature
 643 measurements in the cold plasma environment of Titan: Implications for atmo-
 644 spheric escape. *Geophys. Res. Lett.*, *37*, 20105. doi: 10.1029/2010GL044544
- 645 Felici, M., Arridge, C. S., Wilson, R. J., Coates, A. J., Thomsen, M., & Reisen-
 646 field, D. (2018). Survey of thermal plasma composition in saturn's magne-
 647 tosphere using time-of-flight data from cassini/caps. *Journal of Geophysi-
 648 cal Research: Space Physics*, *123*(8), 6494-6513. Retrieved from <https://agupubs.onlinelibrary.wiley.com/doi/abs/10.1029/2017JA025085> doi:
 649 10.1029/2017JA025085
- 651 Garnier, P., Dandouras, I., Toubanc, D., Roelof, E. C., Brandt, P. C., Mitchell,
 652 D. G., ... Wahlund, J.-E. (2010, December). Statistical analysis of the en-
 653 ergetic ion and ENA data for the Titan environment. *Planet. Space Sci.*, *58*,
 654 1811-1822. doi: 10.1016/j.pss.2010.08.009
- 655 Gurnett, D. A., Kurth, W. S., Kirchner, D. L., Hospodarsky, G. B., Averkamp,
 656 T. F., Zarka, P., ... Pedersen, A. (2004, September). The Cassini Radio
 657 and Plasma Wave Investigation. *Space Science Reviews*, *114*, 395-463. doi:
 658 10.1007/s11214-004-1434-0
- 659 Halekas, J. S., Brain, D. A., Luhmann, J. G., DiBraccio, G. A., Ruhunusiri, S.,
 660 Harada, Y., ... Jakosky, B. M. (2017). Flows, fields, and forces in the mars-
 661 solar wind interaction. *Journal of Geophysical Research: Space Physics*,
 662 *122*(11), 11,320-11,341. Retrieved from <https://agupubs.onlinelibrary.wiley.com/doi/abs/10.1002/2017JA024772> doi: 10.1002/2017JA024772
- 664 Hartle, R. E., Sarantos, M., & Sittler, E. C., Jr. (2011, October). Pickup ion distri-
 665 butions from three-dimensional neutral exospheres. *Journal of Geophysical Re-
 666 search (Space Physics)*, *116*(A15), 10101. doi: 10.1029/2011JA016859
- 667 Hartle, R. E., & Sittler, E. C. (2007, July). Pickup ion phase space distributions: Ef-
 668 fects of atmospheric spatial gradients. *Journal of Geophysical Research (Space*

- 669 *Physics*), 112, 7104. doi: 10.1029/2006JA012157
- 670 Hartle, R. E., Sittler, E. C., Neubauer, F. M., Johnson, R. E., Smith, H. T., Crary,
671 F., ... Andre, N. (2006, April). Preliminary interpretation of Titan plasma in-
672 teraction as observed by the Cassini Plasma Spectrometer: Comparisons with
673 Voyager 1. *Geophys. Res. Lett.*, 33, 8201-+. doi: 10.1029/2005GL024817
- 674 Hartle, R. E., Sittler, E. C., Ogilvie, K. W., Scudder, J. D., Lazarus, A. J., &
675 Atreya, S. K. (1982, March). Titan's ion exosphere observed from Voyager
676 1. *J. Geophys. Res.*, 87, 1383-1394. doi: 10.1029/JA087iA03p01383
- 677 Ledvina, S. A., Brecht, S. H., & Cravens, T. E. (2012, February). The orientation of
678 Titan's dayside ionosphere and its effects on Titan's plasma interaction. *Earth,*
679 *Planets, and Space*, 64, 207-230. doi: 10.5047/eps.2011.08.009
- 680 Lewis, G. R., André, N., Arridge, C. S., Coates, A. J., Gilbert, L. K., Linder, D. R.,
681 & Rymer, A. M. (2008, May). Derivation of density and temperature from the
682 Cassini Huygens CAPS electron spectrometer. *Planet. Space Sci.*, 56, 901-912.
683 doi: 10.1016/j.pss.2007.12.017
- 684 Luhmann, J. G. (1996). Titan's ion exosphere wake: A natural ion mass spec-
685 trometer? *Journal of Geophysical Research: Planets*, 101(E12), 29387-29393.
686 Retrieved from [https://agupubs.onlinelibrary.wiley.com/doi/abs/](https://agupubs.onlinelibrary.wiley.com/doi/abs/10.1029/96JE03307)
687 [10.1029/96JE03307](https://agupubs.onlinelibrary.wiley.com/doi/abs/10.1029/96JE03307) doi: 10.1029/96JE03307
- 688 Ma, Y., Nagy, A. F., Cravens, T. E., Sokolov, I. V., Hansen, K. C., Wahlund, J.-E.,
689 ... Dougherty, M. K. (2006, May). Comparisons between MHD model cal-
690 culations and observations of Cassini flybys of Titan. *Journal of Geophysical*
691 *Research (Space Physics)*, 111, 5207. doi: 10.1029/2005JA011481
- 692 Modolo, R., & Chanteur, G. M. (2008, January). A global hybrid model for Titan's
693 interaction with the Kronian plasma: Application to the Cassini Ta flyby. *J.*
694 *Geophys. Res.*, 113(A12), 1317-+. doi: 10.1029/2007JA012453
- 695 Modolo, R., Chanteur, G. M., Wahlund, J.-E., Canu, P., Kurth, W. S., Gurnett, D.,
696 ... Bertucci, C. (2007). Plasma environment in the wake of titan from hybrid
697 simulation: A case study. *Geophysical Research Letters*, 34(24). Retrieved
698 from [https://agupubs.onlinelibrary.wiley.com/doi/abs/10.1029/](https://agupubs.onlinelibrary.wiley.com/doi/abs/10.1029/2007GL030489)
699 [2007GL030489](https://agupubs.onlinelibrary.wiley.com/doi/abs/10.1029/2007GL030489) doi: 10.1029/2007GL030489
- 700 Modolo, R., Wahlund, J., Boström, R., Canu, P., Kurth, W. S., Gurnett, D.,
701 ... Coates, A. J. (2007, October). Far plasma wake of Titan from the

- 702 RPWS observations: A case study. *Geophys. Res. Lett.*, *34*, 24-+. doi:
703 10.1029/2007GL030482
- 704 Morooka, M., Modolo, R., Wahlund, J. E., André, M., Eriksson, A. I., Persoon,
705 D. A., A. M. and Gurnett, ... Dougherty, M. (2009). The electron den-
706 sity of Saturn's magnetosphere. *Annales Geophysicae*, *27*, 2971-2991. doi:
707 10.5194/angeo-27-2971-2009
- 708 Nelson, D., & Berthelier, J. J. (2009). *Caps simulator, handbook* (Tech. Rep.). LAT-
709 MOS.
- 710 Neubauer, F. M., Backes, H., Dougherty, M. K., Wennmacher, A., Russell, C. T.,
711 Coates, A., ... Saur, J. (2006, October). Titan's near magnetotail from
712 magnetic field and electron plasma observations and modeling: Cassini
713 flybys TA, TB, and T3. *J. Geophys. Res.*, *111*(A10), 10220-+. doi:
714 10.1029/2006JA011676
- 715 Németh, Z., Szego, K., Bebesi, Z., Erdős, G., Foldy, L., Rymer, A., ... Wellbrock,
716 A. (2011). Ion distributions of different kronian plasma regions. *Journal*
717 *of Geophysical Research: Space Physics*, *116*(A9). Retrieved from [https://](https://agupubs.onlinelibrary.wiley.com/doi/abs/10.1029/2011JA016585)
718 agupubs.onlinelibrary.wiley.com/doi/abs/10.1029/2011JA016585 doi:
719 10.1029/2011JA016585
- 720 Regoli, L. H., Coates, A. J., Thomsen, M. F., Jones, G. H., Roussos, E., Waite,
721 J. H., ... Cox, G. (2016, September). Survey of pickup ion signatures in the
722 vicinity of Titan using CAPS/IMS. *Journal of Geophysical Research (Space*
723 *Physics)*, *121*, 8317-8328. doi: 10.1002/2016JA022617
- 724 Regoli, L. H., Roussos, E., Dialynas, K., Luhmann, J. G., Sergis, N., Jia, X.,
725 ... Rae, I. J. (2018). Statistical study of the energetic proton environ-
726 ment at titan's orbit from the cassini spacecraft. *Journal of Geophysical*
727 *Research: Space Physics*, *123*(6), 4820-4834. Retrieved from [https://](https://agupubs.onlinelibrary.wiley.com/doi/abs/10.1029/2018JA025442)
728 agupubs.onlinelibrary.wiley.com/doi/abs/10.1029/2018JA025442 doi:
729 10.1029/2018JA025442
- 730 Romanelli, N., Bertucci, C., Gómez, D., Mazelle, C., & Delva, M. (2013, February).
731 Proton cyclotron waves upstream from Mars: Observations from Mars Global
732 Surveyor. *Planet. Space Sci.*, *76*, 1-9. doi: 10.1016/j.pss.2012.10.011
- 733 Romanelli, N., Modolo, R., Dubinin, E., Berthelier, J.-J., Bertucci, C., Wahlund,
734 J. E., ... Dougherty, M. (2014). Outflow and plasma acceleration in titan's

- 735 induced magnetotail: Evidence of magnetic tension forces. *Journal of Geophys-*
 736 *ical Research: Space Physics*, 119(12), 9992-10,005. Retrieved from [https://](https://agupubs.onlinelibrary.wiley.com/doi/abs/10.1002/2014JA020391)
 737 agupubs.onlinelibrary.wiley.com/doi/abs/10.1002/2014JA020391 doi:
 738 10.1002/2014JA020391
- 739 Russell, C. T., Wei, H. Y., Cowee, M. M., Neubauer, F. M., & Dougherty, M. K.
 740 (2016). Ion cyclotron waves at titan. *Journal of Geophysical Research: Space*
 741 *Physics*, 121(3), 2095-2103. Retrieved from [https://agupubs.onlinelibrary](https://agupubs.onlinelibrary.wiley.com/doi/abs/10.1002/2015JA022293)
 742 [.wiley.com/doi/abs/10.1002/2015JA022293](https://agupubs.onlinelibrary.wiley.com/doi/abs/10.1002/2015JA022293) doi: 10.1002/2015JA022293
- 743 Rymer, A. M., Smith, H. T., Wellbrock, A., Coates, A. J., & Young, D. T. (2009,
 744 August). Discrete classification and electron energy spectra of Titan's var-
 745 ied magnetospheric environment. *Geophys. Res. Lett.*, 36, 15109-+. doi:
 746 10.1029/2009GL039427
- 747 Sillanpää, I., Kallio, E., Janhunen, P., Schmidt, W., Mursula, K., Vilppola, J., &
 748 Tanskanen, P. (2006). Hybrid simulation study of ion escape at Titan for
 749 different orbital positions. *Advances in Space Research*, 38, 799-805. doi:
 750 10.1016/j.asr.2006.01.005
- 751 Simon, S., Boesswetter, A., Bagdonat, T., Motschmann, U., & Schuele, J. (2007,
 752 February). Three-dimensional multispecies hybrid simulation of Titan's highly
 753 variable plasma environment. *Annales Geophysicae*, 25, 117-144.
- 754 Simon, S., Neubauer, F. M., Wennmacher, A., & Dougherty, M. K. (2014, March).
 755 Variability of Titan's induced magnetotail: Cassini magnetometer observa-
 756 tions. *Journal of Geophysical Research (Space Physics)*, 119, 2024-2037. doi:
 757 10.1002/2013JA019608
- 758 Simon, S., van Treeck, S. C., Wennmacher, A., Saur, J., Neubauer, F. M., Bertucci,
 759 C. L., & Dougherty, M. K. (2013). Structure of titan's induced magne-
 760 tosphere under varying background magnetic field conditions: Survey of
 761 cassini magnetometer data from flybys ta-t85. *Journal of Geophysical*
 762 *Research: Space Physics*, 118(4), 1679-1699. Retrieved from [https://](https://agupubs.onlinelibrary.wiley.com/doi/abs/10.1002/jgra.50096)
 763 agupubs.onlinelibrary.wiley.com/doi/abs/10.1002/jgra.50096 doi:
 764 10.1002/jgra.50096
- 765 Simon, S., Wennmacher, A., M., N., Bertucci, C. L., Kriegel, H., Saur, J., ...
 766 Dougherty, M. K. (2010). Titan's highly dynamicmagnetic environment :
 767 A systematic survey of cassini magnetometer observations from flybys ta-t62.

- 768 *Planet. Space Sci.* doi: 10.1016/j.pss.2010.04.021
- 769 Sittler, E. C., Hartle, R. E., Johnson, R. E., Cooper, J. F., Lipatov, A. S., Bertucci,
770 C., . . . Wahlund, J.-E. (2010, February). Saturn’s magnetospheric interaction
771 with Titan as defined by Cassini encounters T9 and T18: New results. *Planet.*
772 *Space Sci.*, *58*, 327-350. doi: 10.1016/j.pss.2009.09.017
- 773 Snowden, D., Winglee, R., Bertucci, C., & Dougherty, M. (2007, December).
774 Three-dimensional multifluid simulation of the plasma interaction at Titan.
775 *Journal of Geophysical Research (Space Physics)*, *112*(A11), 12221. doi:
776 10.1029/2007JA012393
- 777 Szego, K., Bebesi, Z., Bertucci, C., Coates, A. J., Crary, F., Erdos, G., . . . Young,
778 D. T. (2007, November). Charged particle environment of Titan during the T9
779 flyby. *Geophys. Res. Lett.*, *34*, 24-+. doi: 10.1029/2007GL030677
- 780 Thomsen, M. F., Reisenfeld, D. B., Delapp, D. M., Tokar, R. L., Young, D. T.,
781 Crary, F. J., . . . Williams, J. D. (2010). Survey of ion plasma parameters
782 in saturn’s magnetosphere. *Journal of Geophysical Research: Space Physics*,
783 *115*(A10). Retrieved from <https://agupubs.onlinelibrary.wiley.com/doi/abs/10.1029/2010JA015267> doi: 10.1029/2010JA015267
- 784
785 Thomsen, M. F., Reisenfeld, D. B., Wilson, R. J., Andriopoulou, M., Crary, F. J.,
786 Hospodarsky, G. B., . . . Tokar, R. L. (2014). Ion composition in inter-
787 change injection events in saturn’s magnetosphere. *Journal of Geophysi-*
788 *cal Research: Space Physics*, *119*(12), 9761-9772. Retrieved from [https://](https://agupubs.onlinelibrary.wiley.com/doi/abs/10.1002/2014JA020489)
789 agupubs.onlinelibrary.wiley.com/doi/abs/10.1002/2014JA020489 doi:
790 10.1002/2014JA020489
- 791 Tokar, R. L., Wilson, R. J., Johnson, R. E., Henderson, M. G., Thomsen, M. F.,
792 Cowee, M. M., . . . Smith, H. T. (2008, July). Cassini detection of water-group
793 pick-up ions in the Enceladus torus. *Geophys. Res. Lett.*, *35*, 14202. doi:
794 10.1029/2008GL034749
- 795 Wahlund, J.-E., Boström, R., Gustafsson, G., Gurnett, D. A., Kurth, W. S., Ped-
796 ersen, A., . . . Müller-Wodarg, I. (2005, May). Cassini Measurements
797 of Cold Plasma in the Ionosphere of Titan. *Science*, *308*, 986-989. doi:
798 10.1126/science.1109807
- 799 Wahlund, J.-E., Modolo, R., Bertucci, C., & Coates, A. (2014). Titan’s Mag-
800 netospheric and Plasma Environment. In I. Müller-Wodarg, C. A. Griffith,

- 801 E. Lellouch, & T. E. Cravens (Eds.), *Titan: Surface, Atmosphere and Magne-*
802 *tosphere*. Cambridge University Press.
- 803 Waite, J. H., Lewis, W. S., Kasprzak, W. T., Anicich, V. G., Block, B. P., Cravens,
804 T. E., ... Yelle, R. V. (2004, September). The Cassini Ion and Neu-
805 tral Mass Spectrometer (INMS) Investigation. , *114*(1-4), 113-231. doi:
806 10.1007/s11214-004-1408-2
- 807 Westlake, J. H., Paranicas, C. P., Cravens, T. E., Luhmann, J. G., Mandt, K. E.,
808 Smith, H. T., ... Wahlund, J.-E. (2012). The observed composition of ions
809 outflowing from titan. *Geophysical Research Letters*, *39*(19). Retrieved
810 from [https://agupubs.onlinelibrary.wiley.com/doi/abs/10.1029/](https://agupubs.onlinelibrary.wiley.com/doi/abs/10.1029/2012GL053079)
811 [2012GL053079](https://agupubs.onlinelibrary.wiley.com/doi/abs/10.1029/2012GL053079) doi: 10.1029/2012GL053079
- 812 Wilson, R. J., Bagenal, F., & Person, A. M. (2017). Survey of thermal plasma ions
813 in saturn's magnetosphere utilizing a forward model. *Journal of Geophysical*
814 *Research: Space Physics*, *122*(7), 7256-7278. Retrieved from [https://agupubs](https://agupubs.onlinelibrary.wiley.com/doi/abs/10.1002/2017JA024117)
815 [.onlinelibrary.wiley.com/doi/abs/10.1002/2017JA024117](https://agupubs.onlinelibrary.wiley.com/doi/abs/10.1002/2017JA024117) doi: 10.1002/
816 [2017JA024117](https://agupubs.onlinelibrary.wiley.com/doi/abs/10.1002/2017JA024117)
- 817 Wilson, R. J., Crary, F., Gilbert, L. K., Reisenfeld, D. B., Steinberg, J. T., & Livi,
818 R. (2012). Pds user's guide for cassini plasma spectrometer. *PDS*. Retrieved
819 from <https://pds-ppi.igpp.ucla.edu/>
- 820 Yokota, S., Saito, Y., Asamura, K., Tanaka, T., Nishino, M. N., Tsunakawa, H., ...
821 Terasawa, T. (2009, June). First direct detection of ions originating from the
822 Moon by MAP-PACE IMA onboard SELENE (KAGUYA). *Geophys. Res.*
823 *Lett.*, *36*, 11201. doi: 10.1029/2009GL038185
- 824 Young, D. T., Berthelier, J. J., Blanc, M., Burch, J. L., Coates, A. J., Goldstein, R.,
825 ... Zinsmeyer, C. (2004, September). Cassini Plasma Spectrometer Investiga-
826 tion. *Space Science Reviews*, *114*, 1-112. doi: 10.1007/s11214-004-1406-4